REPORT DOCUMENTATION PAGE

Form Approved OMB No. 0704-0188

1. REPORT DATE *(DD-MM-YYYY)*	2. REPORT TYPE	3. DATES COVERED *(From – To)*
23-04-2007	Final Report	4 July 2003 - 19-May-07

4. TITLE AND SUBTITLE

Electron Beam Control of Combustion

5a. CONTRACT NUMBER
FA8655-03-D-0001, Delivery Order 0011

5b. GRANT NUMBER

5c. PROGRAM ELEMENT NUMBER

6. AUTHOR(S)

Dr. Georgy Pozdnyakov

5d. PROJECT NUMBER

5d. TASK NUMBER

5e. WORK UNIT NUMBER

7. PERFORMING ORGANIZATION NAME(S) AND ADDRESS(ES)

Institute of Theoretical and Applied Mechanics
ul. Institutskaya, 4/1
Novosibirsk 630090
Russia

8. PERFORMING ORGANIZATION REPORT NUMBER

N/A

9. SPONSORING/MONITORING AGENCY NAME(S) AND ADDRESS(ES)

EOARD
PSC 821 BOX 14
FPO AE 09421-0014

10. SPONSOR/MONITOR'S ACRONYM(S)

11. SPONSOR/MONITOR'S REPORT NUMBER(S)
EOARD Task 03-9004

12. DISTRIBUTION/AVAILABILITY STATEMENT

Approved for public release; distribution is unlimited.

13. SUPPLEMENTARY NOTES

14. ABSTRACT

This report results from a contract tasking Institute of Theoretical and Applied Mechanics as follows: The contractor will investigate using an electron beam to ignite and aid combustion in hydrocarbon fuel-air mixtures. The experimental portion of the project will assess the influence of electron beam pulse duration, electron energy density, gas mixture velocity (from quiesent to supersonic), gas mixture constituents, temperature, pressure, and stoichiometry. The contractor will measure the influence on reaction induction time, flame stability, and combustion efficiency. In parallel, the contract will develop a kinetic model to assess the theory behind the reactions influenced by the electron beam.

15. SUBJECT TERMS
EOARD, ignition, Combustion, Electron Beam

16. SECURITY CLASSIFICATION OF:			17. LIMITATION OF ABSTRACT	18, NUMBER OF PAGES	19a. NAME OF RESPONSIBLE PERSON
a. REPORT	b. ABSTRACT	c. THIS PAGE			SURYA SURAMPUDI
UNCLAS	UNCLAS	UNCLAS	UL	38	19b. TELEPHONE NUMBER *(Include area code)* +44 (0)20 7514 4299

FINAL TECHNICAL REPORT

ELECTRON BEAM CONTROL OF COMBUSTION

CRDF project # RP0-1393-NO-03
start date is July 4, 2003,
finish date is July 4, 2006.

Principal Organization Institute of Theoretical and Applied Mechanics SB RAS
Project Director Dr. Georgy A. Pozdnyakov

Novosibirsk, 2006

Introduction

During recent decades the processes of combustion in a supersonic stream have been actively studied. It is shown that such combustion can be realized for hydrogen. Stable combustion of kerosene at Mach numbers higher than 2 still has not met with success.

The problem is mainly in the fact that the time of combustion reaction induction is too big as compared to the time of flyby through a reactor.

In the project presented it was supposed to study the process of initiation of carbohydrates combustion with the aid of a high-current electron beam of low energy (about 10 keV), electron density of about $10^{10} \div 10^{11} cm^{-3}$. The experimental data for the kinetics of carbohydrates (including liquid matters) combustion reactions accompanied by the electron beam was obtained; a kinetic model of such reactions was formed. It is anticipated that the application of the electron beam will result in essential decrease of the induction time, flame stabilization, increasing dispersity of the fuel liquid phase. Combustion efficiency growth is expected to increase too. The application of the electron beam for combustion reaction initiating is based on the use of excitation of oscillating levels of gas mixture molecules by electrons which cause reagents activation. It is known that the most effective excitation of the oscillation levels is carried out by low-energy electrons. The application of the electron beam for this purpose is suggested to be more effective as compared to alternative methods of combustion initiation, for instance with the aid of electric discharge or laser emission.

Experimental part.

I. Characteristics of an electron source.

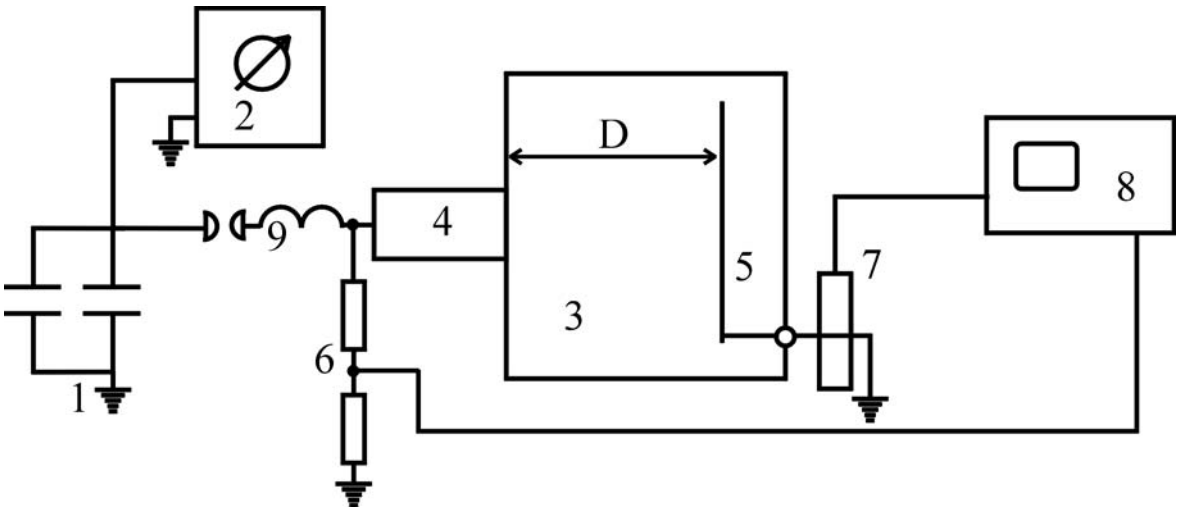

Fig. 1. Sketch of the device for measuring electron gun characteristics

The sketch of the device for measuring electron gun characteristics is presented in Fig.1. The device consists of high-volt capacitor bank 1 with voltage supply 2, vacuum container 3, and electron gun 4 jointed to it. Inside this container there collector 5 sets for full current and current density distribution measurements. The collector inside the container may be set in any distance *D*. The currents are measured by integrating Rogovski coil 7, and registered by digital oscillograph 8. Additional inductivity *L* (9) is intended

for forming current pulses of the electron beam. The voltage divider 6 is intended for measurement of a voltage on an electron gun.

The measurement of a complete electron current was carried out with use of a graphite collector by a diameter 160mm, established on distance *D* of the order of 50 mm from a source. Vacuum volume was pumped out up to pressure 5-6 Pa. The capacitors were charged up to a voltage *U*=22kV. The typical signal from a Rogovsky coil is shown on Fig.2.

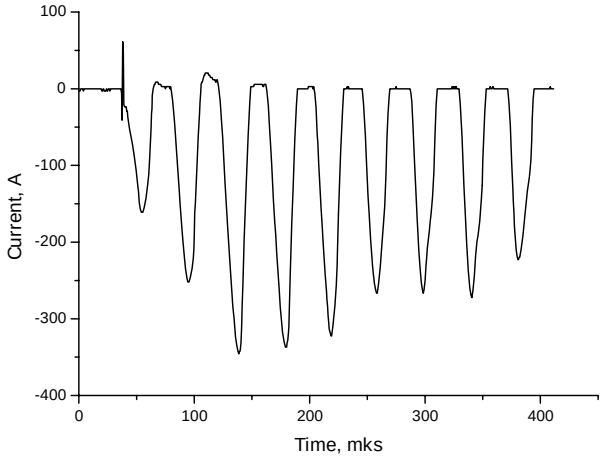

Fig. 2 Full current of the e-beam.

I.1. Measurement of spatial distribution of a current.

The measurements were carried out with the help of a collector, schematic shown on Fig.4. The collector is made from foil-clad textolite. On it's covering 13 current data units with the size 10×10mm was formed . The collector was established on distance 30, 60 and 90 mm from a source. The measurements were carried out by series till 13 experiments. In each experiment the current through one of data units was measured. Other sensors and surface of a collector was grounded. On Fig.3 the average meanings of currents through the appropriate data units received at distance between a collector and the source 90mm are specified. The given data specify that the electron source makes a cloud of electrons with cross section of the order 10 cm.

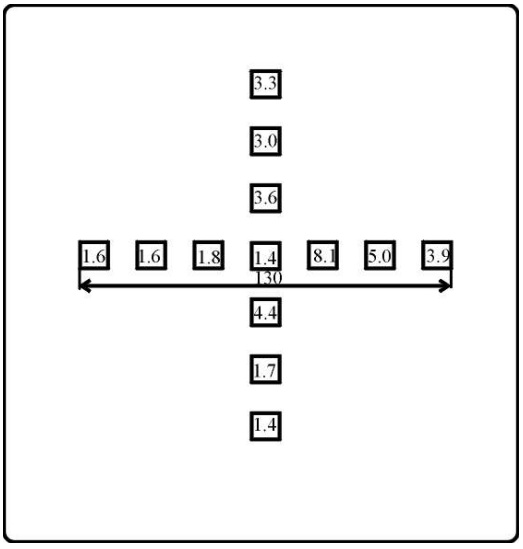

Fig.3. Sketch of the collector for current dencity measurements.

I.2. Measurement of a voltage on the e – source.

The measurement of a voltage on the electron source allows to estimate the maximal probable electrons energy. The signals of a complete current through a collector and voltage on a source are shown in a fig. 4 (L = 0) and Fig.5 (L = 6 mkH). The current was measured with the help of a graphite collector located on distance D = 120mm from a exhaust window of an e – gun. Measurements were carried out at residual pressure of air about 5 Pa. The delay of a collector current from a voltage on a source is connected with electrons diffusion in residual gas. The electrons energy in first pulse can be up to 16 keV.

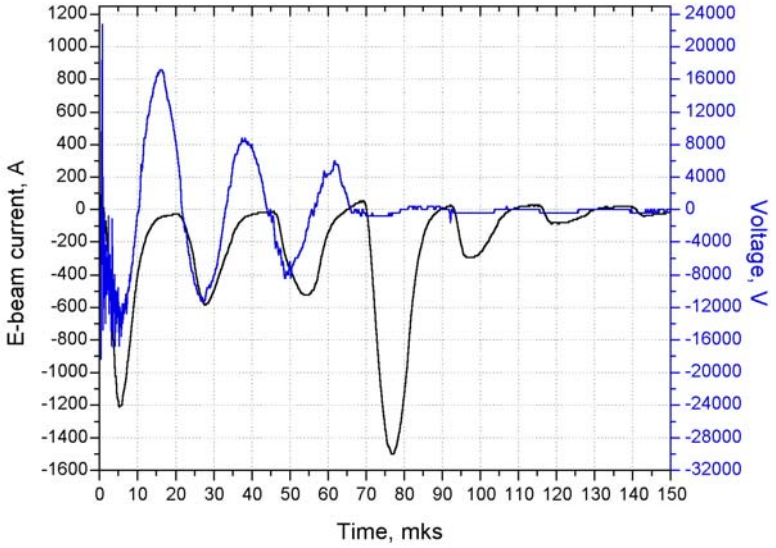

Fig. 4. Signals of complete current and voltage on the e-gun (L=0).

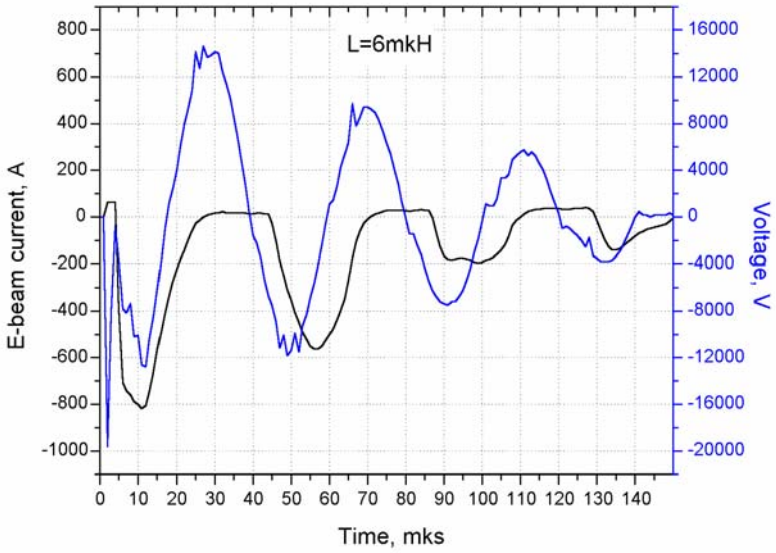

Fig. 5. Signals of complete current and voltage on the e-gun (L=6mkH).

I.3. Full current regarding gas pressure and kind.

The tests of the electron source, the working volume being filled with different gases up to different pressure, have permitted to determine the range of combustible mixtures

working pressures. The tests have been performed with helium as the most probable buffer gas, air (oxidizer), and argon – the gas with a big atomic mass. Fig. 6 – 8 presents the corresponding results.

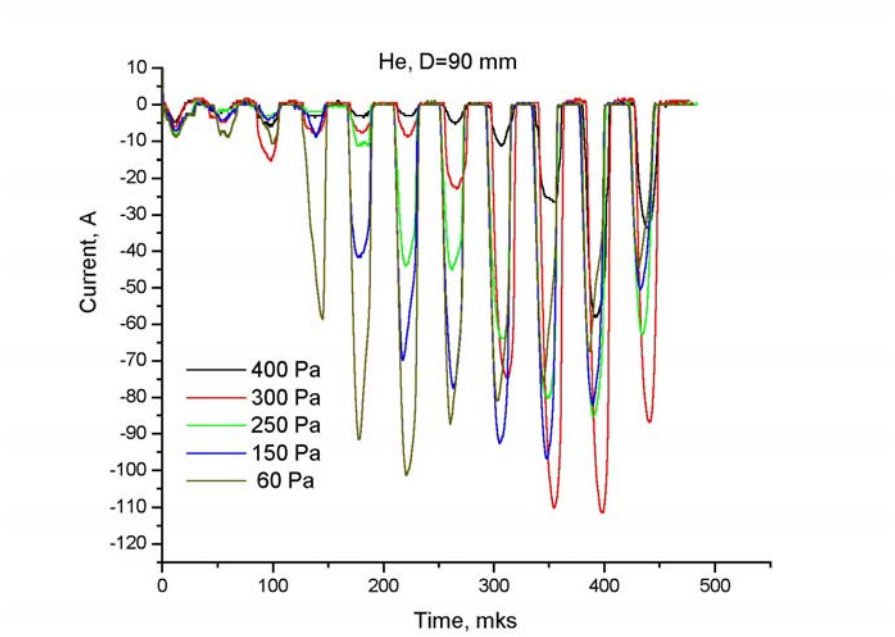

Fig. 6. Complete current in helium

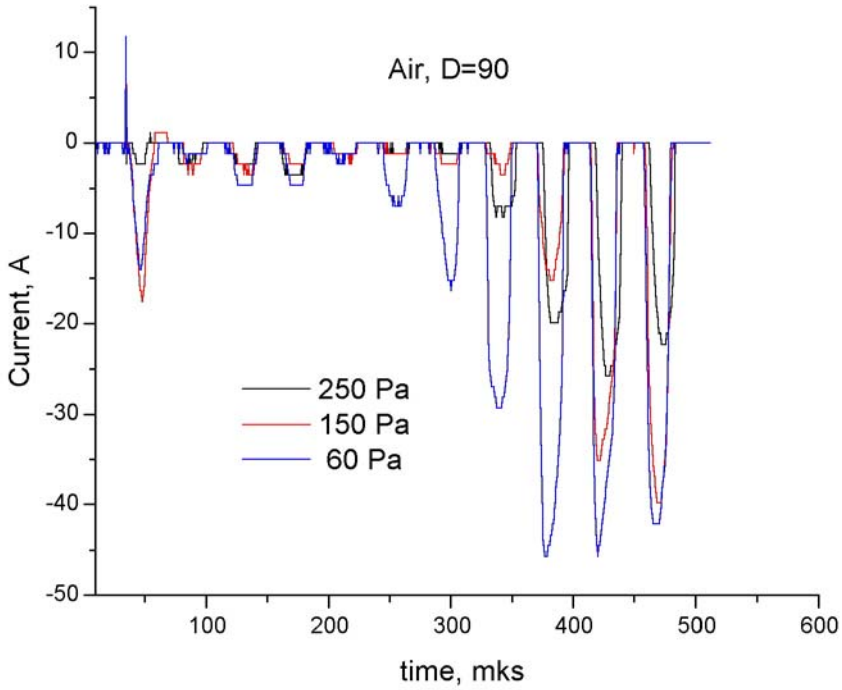

Fig. 7. Complete current in air.

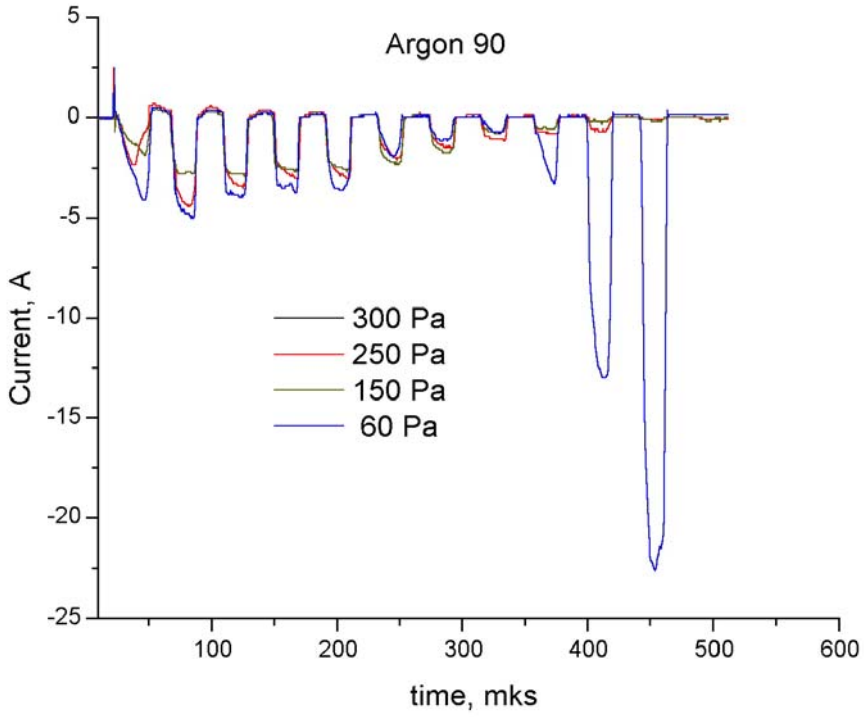

Fig. 8. Complete current in argon.

The graphs presented demonstrate that as the molecular mass rises, the beam current decreases. With the pressure growth, the current maximum is reached with the longer delay as compared to the source start. These graphs also allow concluding that this source can be applied at the air pressure of about 200 Pa.

We obtained following characteristics of e-source:

1. Typical amplitude of an electron current is a few hundreds amperes.
2. The beam cross section has a diameter of more than 10 cm.

This existing source may be used at the combustion reaction pressure up to 200 Pa.

II Experiments with combustion initialization in the rest mixtures.

II.1. Experimental setup and methods of investigations.

Sketch of the installation for investigations with rest gas mixtures is presented in Fig.9, general view of the installation is presented in Fig.10.

The scheme of an experiment is the following:

1. Mounting of a plastic film
2. Evacuation of the experimental cell (not shown) and cell for experimental gas mixture.
3. Filling the cell for experimental gas by gas mixture.
4. Charging of the capacitor C.
5. The start-up is made. The plastic film destroys by impulse current heating wire (not shown). Gas mixture from the cell fills the experimental cell. The start-up of the e-gun is made with 14 ms delay. Measurements of voltage on the gun, e-beam current, light radiation (complete or in any emission band) are executes.

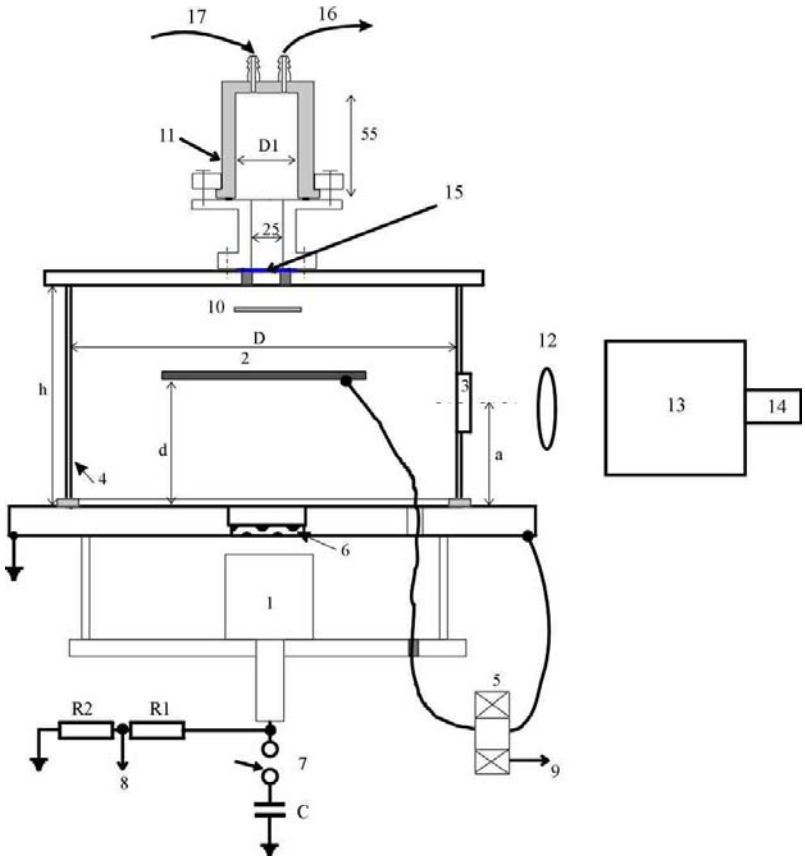

Fig. 9. The experimental cell. *1*- electron gun, *2*- electron collector, *3* – quartz window, *4* – cylindrical wall of the cell, *5* – Rogowsky coil, *6* – perforated exhaust window for e-beam, *7* - discharger, *8,9* – to voltage and current registration, *10* - impingement plate, *11* – cell with experimental gas mixture, *12* – quartz lens, *13* – monochromator, *14* - photomultiplier tube, *15* – plastic film, *16* – cell evacuation, *17* – cell filling.

Fig.10. The general view of the experimental installation. *1* – experimental cell, *2* – cell for experimental gas mix, *3* – quartz lens, *4* – monochromator, *5* – impulse current generator for plastic film destroy, *6* – device for mix preparing, *7* – gas balloon, *8* – cable for e-gun feeding, *9* – vacuum pump.

II. 2 Initiation of the hydrogen-oxygen reactions.

Control of hydrogen combustion in oxygen was studied for beginning. The time dependencies of the radiation intensity were registered on different wavelengths, they were synchronized with the electron gun.

To choose the operation spectrum interval, and to adjust the monochromator, we registered a spectrum of hydrogen-air flame radiation. Fig. 11 shows the spectrum of hydrogen-air flame, obtained by scanning the working area of the monochromator. In the spectrum two peaks are seen – near the wavelength of 300 nm and 590 nm. The latter belongs to sodium doublet, which always exists in air in dust. The first one is observed in the flame of the hydrocarbon fuel.

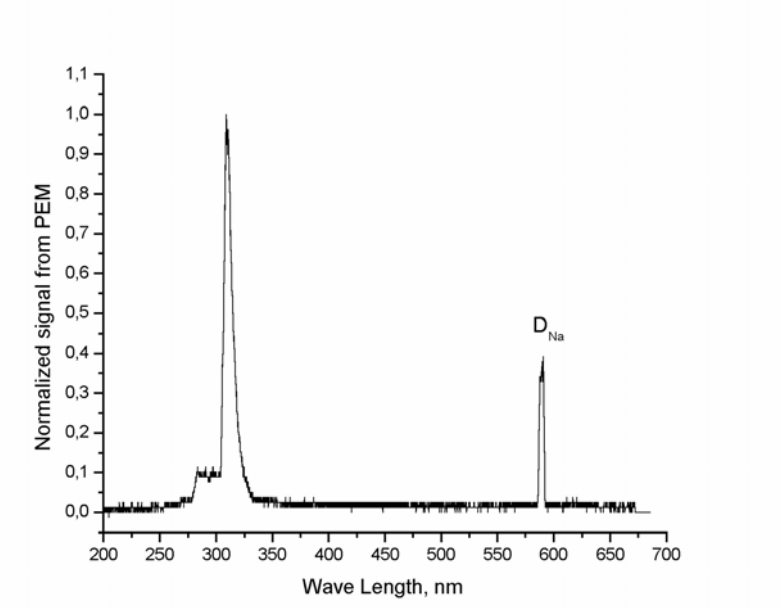

Fig. 11. Spectrum of hydrogen-air flame, obtained by scanning of the monochromator working area. The detector was a photo-electronic multiplier, sensitive in the region of wavelength of more than 250 nm.

The experiments on hydrogen combustion initiating involved the synchronic registration of the electron-beam current and the intensity of glow of the irradiation region. The pressure of the working medium was of 200 Pa. The measured brightness of the glow presented in Fig. 12, were obtained for λ = 310 nm. The share of oxygen rising, the brightness of the line decreases, and the delay with respect to the effect grows, the half-width rises.

Under the conditions of our experiments, the time of induction of the combustion reaction should be counted from the moment of radiation ceasing, since while the electron gun operates, the reaction does not perform, and the time of the gun operation can be short enough. Then, basing on the intensity level of 0.2, the induction time can be assumed of about 250 microseconds for the stoichiometry mixture.

The radiation of molecular hydrogen is apparently registered here, since the radiation from this wavelength is observed under the e-beam action on pure hydrogen, too.

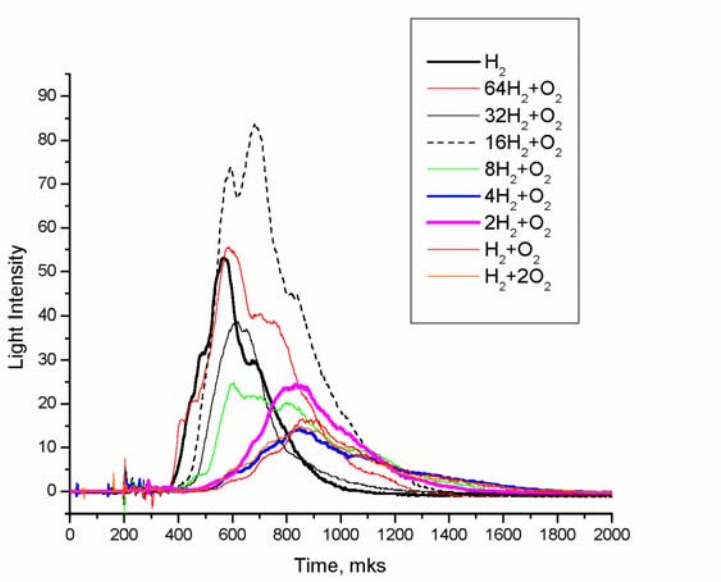

Fig. 12. The intensity of line glow λ = 310 nm depending on time for different mixtures. The radiation is started in the time point of t = 200 microseconds, the duration of electron action is about 150 microseconds. A crimson curve corresponds to the stoichiometry mixture

It is interesting that the combustion starts after the ceasing of electron-radiation of the mixture. In this connection we assumed that molecules dissociate under the electron irradiation, and we should observe the radiation of atoms of, for example, hydrogen, during the irradiation. To test this assumption, we performed a series of experiments to observe the time dependence of the irradiation line H_γ. Fig. 13 and 14 present the corresponding oscillograms for the stoichiometry mixture, synchronized with the electron current passing through the mixture. We observed two peaks of irradiation intensity. The first one is related to the hydrogen atom irradiation, the atoms resulted from the molecular hydrogen dissociation. Fig. 14 presents the oscillogram of this peak with higher resolution, and it is seen that the glow intensity correlates with the amplitude of the electron current. The second peak correlates with the irradiation of λ = 310 nm and is evidently related to the irradiation of the hydrogen atoms involved in the chain combustion reaction.

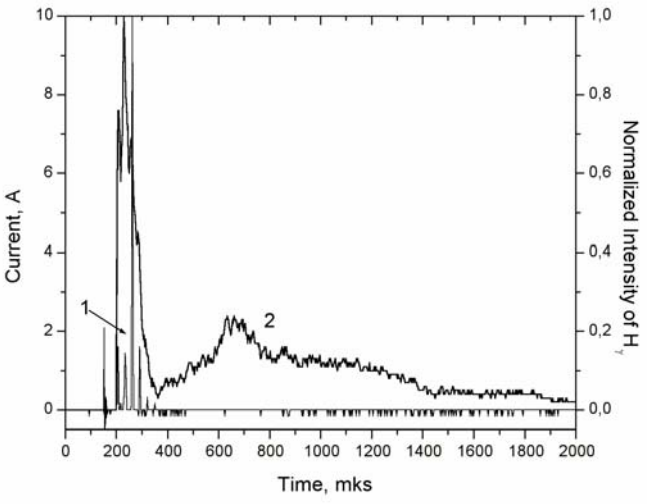

Fig. 13. Intensity of atomic hydrogen line H_γ, normalized for maximum (2), and synchronic – the amplitude of the collector current (the current passing through the mixture and captured in the collector) (1). Stoichiometry mixture.

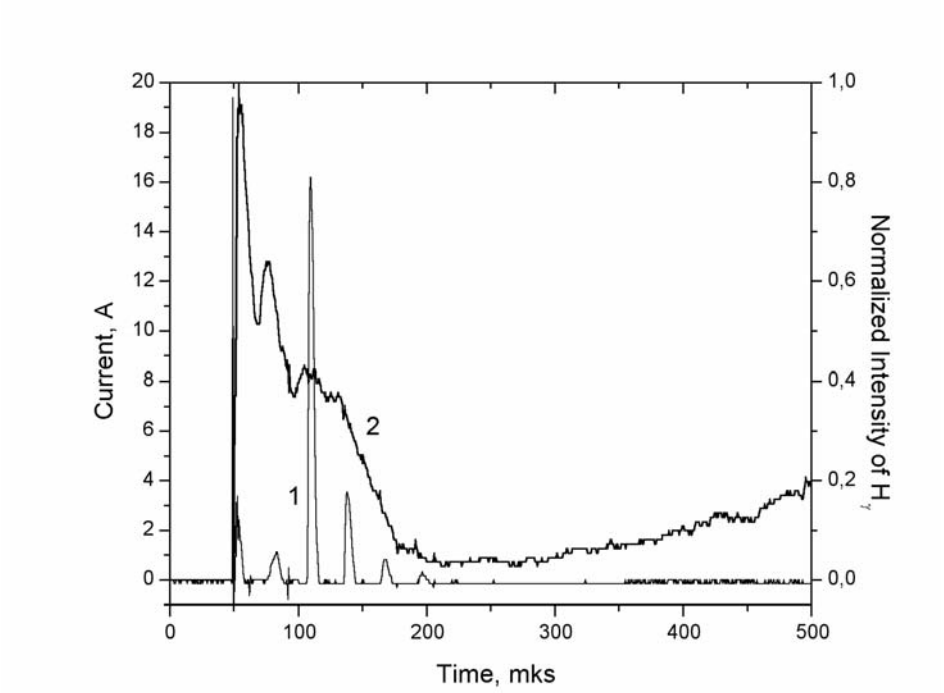

Fig. 14. Same experimental conditions as in Fig. 13, the time discretization is less.

.

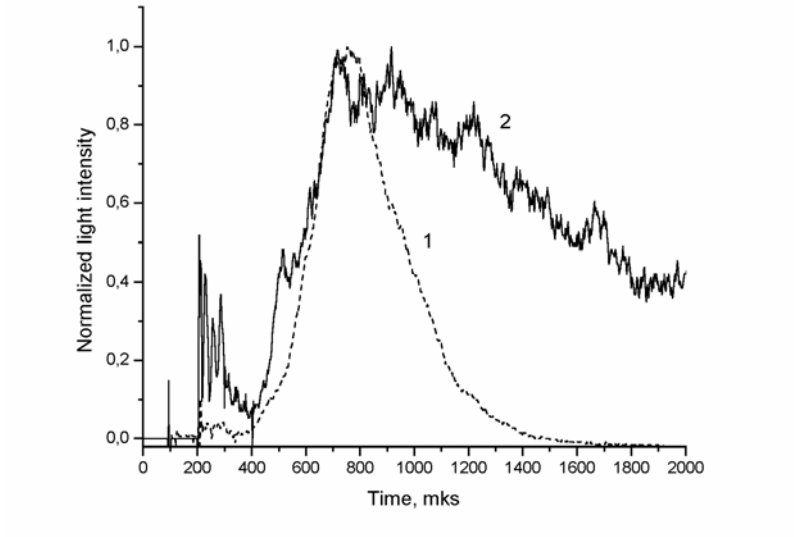

Fig. 15. Normalized dependencies of the intensities of molecular hydrogen lines (1) and sodium doublet 589 nm (2) on time

To prove the possibility of initiating of the combustion reaction by the electron beam, the time dependence of the sodium doublet glow was registered. The intensity of the double glow depends monotonically on the temperature in our temperature range (up to 3000 K). The glow of the sodium doublet was observed for the stoichiometry mixture. Fig. 15 shows this dependence combined with the dependence of the hydrogen line taken

from Fig. 11 (stoichiometry mixture). Sodium was not introduced expressly, it is always contained by gases in trace amount.

The combustion reaction develops after the end of the electron radiation of the mixture, and runs up during the time of about 500 microseconds, the induction time about 100 – 200 microseconds. Then the gas cools slowly, which is vindicated by the slow decrease of the sodium doublet intensity.

II.3 Initiation of hydrocarbon fuel combustion in oxygen and air.

Previously the spectra of natural gas flames (methane was more than 95%), or propane-butane mixture, and petroleum were registered in the air. Fig. 16 shows the qualitative identity of the spectra of flame cores radiation. A peak about 310 nm, typical for a hydrogen-air flame, is seen during the whole jet length. Basing on the results of experiments with hydrogen from the last quarter, we suppose that here we observe the radiation of hydrogen molecules excited by the association of $H + H \rightarrow H_2^*$. The line of 590 nm corresponds to a *Na* doublet, and exists in each spectrum. The rest peaks are related to the radiation of the excited intermediates.

The performance of the experiment on electron-beam initiation of the reactions is similar to the previous one, which was described in the *II.2* part of this report. The time of beam operation is slightly shorter– 10^{-4}s instead of 1.5×10^{-4}s.

We used the radiation with the wavelength of about 310 nm as an indicator of the combustion reaction for each fuel under study. For the reaction of combustion of a stochiometric methane-oxygen mixture, Fig. 17 presents the dependencies of this radiation on time, the moment of beam start corresponds to 0.1 ms. The time dependence

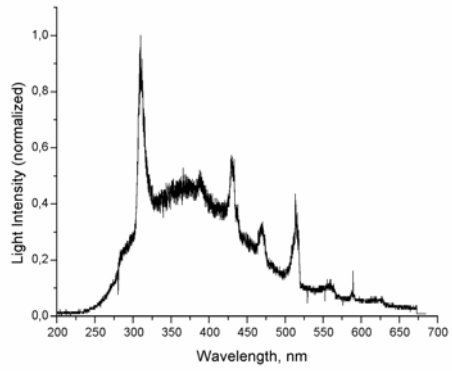

Propane – butane in a flame cone behind a gas jet nozzle (at 15mm).

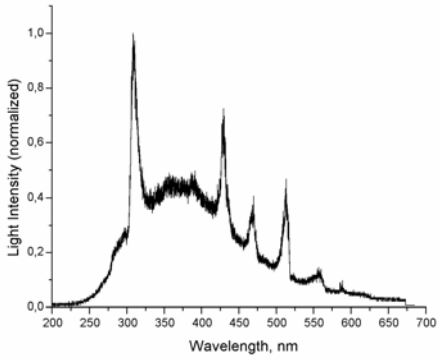

Propane – butane in a flame cone at 50mm

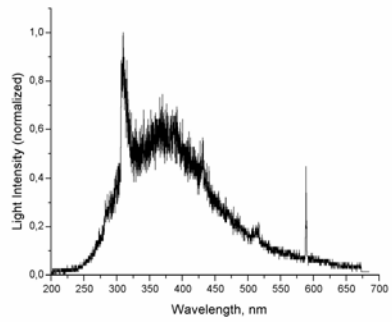

Propane – butane behind a flame cone

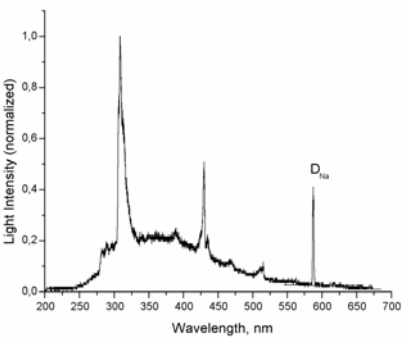

Natural gas in a flame cone

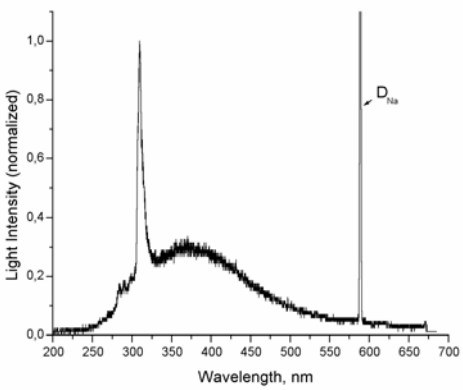

Natural gas behind a flame cone

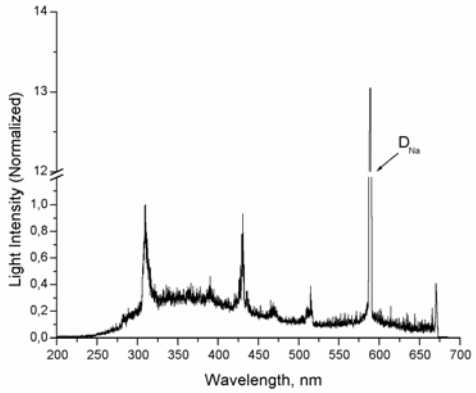

Spectrum of a flame of the petrol torch

Fig. 16 Spectra of different flames of a gas jet and a petrol torch.

of the glow from the reaction region for the natural gas repeats qualitatively, there are some (6) evident maximums, whereas in the case of hydrogen only one maximum is observed, the time of reaction being similar. This difference may result from the generation of intermediate products during the oxidation reactions. These intermediate products may include both different radicals and hydrocarbons with the structure more intricate than methane has. The consequent detachment of hydrogen atoms from these intermediates perhaps leads to the discovered dependence. The investigation of this effect is likely to present an individual task. The basic property of the natural gas combustion is that the inductance time of this reaction is essentially less than in the case of $2H_2+O_2$ reaction.

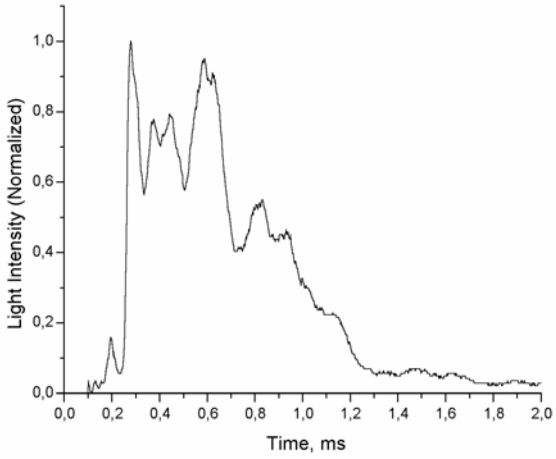

Fig. 17. The intensity of light radiation at 310 nm depending on time for stochiometric mixture of methane and oxygen (CH_4+2O_2).

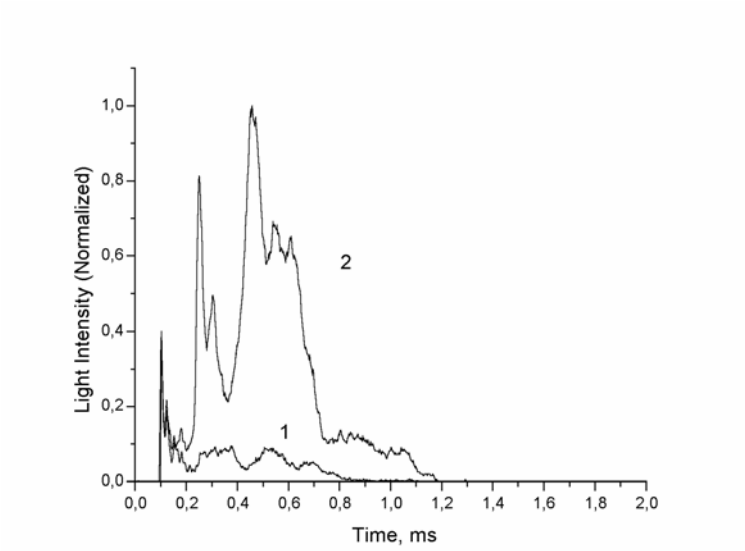

Fig. 18. The intensity of light radiation on 310 nm depending on time for *1* – methane, *2* – rich ($5CH_4+O_2$) mixture of methane and oxygen.

Fig. 18 presents the time dependencies of the radiation intensity for a rich mixture (oxygen concentration is 10 times less than for the stochiometric mixture). The graph had almost no qualitative changes. The reaction time reduced approximately 1.5 times, it also reduced in the case of the rich hydrogen-oxygen mixture. This is seemingly caused by the fact that the reaction occurs in the whole volume at once, and all oxygen is involved in the reaction by this moment. The same graph shows the time dependence of the glow intensity after the electron beam action for the pure natural gas. When the common glow intensity is less, the qualitative similarity of the behavior of the dependence of the glow intensity on time is observed. During the electron gun operation (up to 0.2 ms), both curves almost coincide, excluding one small peak in the are of 0.15 ms. This means, that the combustion reaction does not occur when the electron gun works. Then one can see the maximums, which may be related to the reacting natural gas and residue oxygen of air, since before the reaction the working volume was pumped-out up to the pressure of about 10 Pa, or less somehow, which makes the order of 1% from the working pressure after the working mixture letting to working volume.

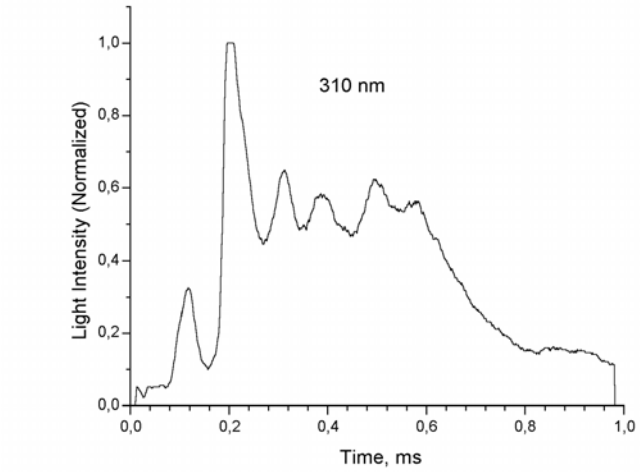

Fig. 19. The intensity of light radiation at 310 nm depending on time for near stochiometric mixture of kerosene and oxygen.

The experiments on kerosene vapor ignition by the electron beam were performed as follows. After the pumping-out of the working chamber, the for-vacuum pump was cut off. The kerosene solution in vacuum oil (1 – 2 ml) was injected into the working volume. In 1 – 2 minutes the whole kerosene was evaporated from the oil, and then was the start – the diaphragm, dividing the working volume and oxygen (or air) capacity, was broken, the oxidizer mixed with the kerosene vapors. The gun was started in 15 ms. The radiation was registered either at the wave length of 310 nm, or in the sodium doublet region of 590 nm. The amount of injected kerosene was controlled by the solution concentration and volume.

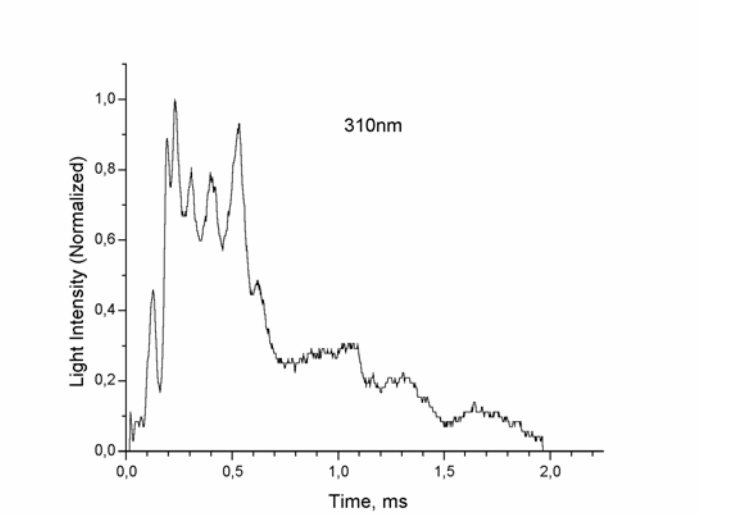

Fig. 20. The intensity of light radiation at 310 nm depending on time for rich mixture of kerosene and oxygen.

Fig. 19 shows the time dependence of the glow intensity of the reaction region in the field of wavelengths of about 310 nm, for the kerosene-oxygen mixture. The moment of electron gun connection almost coincides with the time zero. The mixture compound approaches stoichiometric. The reaction inductance time is the same as for the natural gas combustion reaction. In each experiment with the kerosene combustion one can observe the same 6 maximums of the time dependence of the radiation intensity with $\lambda \approx 310$ nm. Fig. 20 presents a similar dependence for the enriched mixture (6 times more kerosene than in last case). The qualitative difference is weak, inductance time is the same.

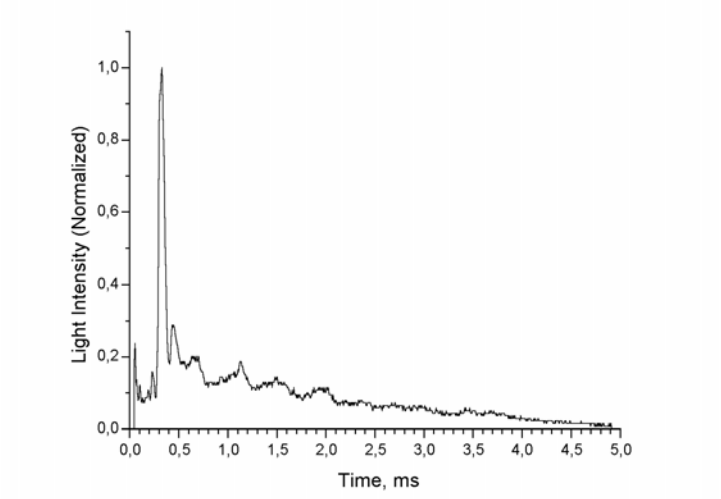

Fig. 21. The intensity of sodium doublet depending on time for kerosene – oxygen mixture.

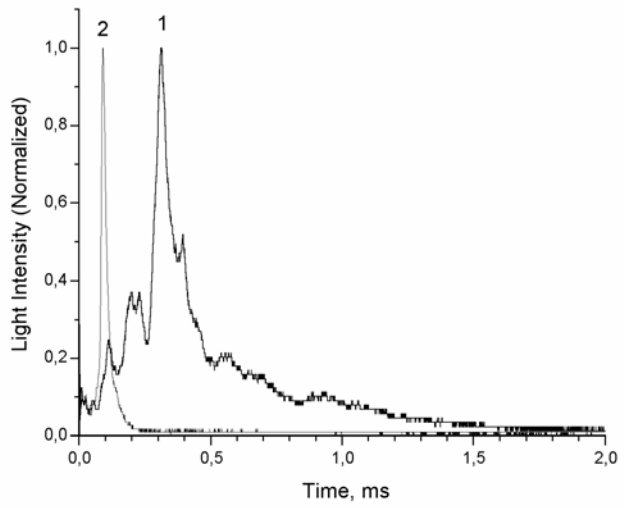

Fig. 22. The intensity of sodium doublet depending on time for kerosene – air mixture (1) and for kerosene vapor (2).

The time dependence of the sodium doublet, shown in Fig. 21, is qualitatively different (the same experiment conditions as in Fig. 19). The radiation pulse is shorter, one major peak is observed, and it approximately corresponds in time to the third maximum in Fig. 19. The side maximums are much less. If we assume that the doublet radiation intensity depends on the temperature of the reacting mixture (if this mixture exists in terms of a local thermodynamic equilibrium), or on the rate of an energy release resulting from the reaction, the time of the energy release resulting from the reaction depends basically on the width of this peak. Further researches must be directed to the more detailed study of this reaction kinetics. Fig. 22 shows a similar dependence (1) for the kerosene-air mixture. The same graph demonstrates a time dependence of the sodium doublet intensity under the action of the electron beam on the kerosene vapors (2). This graph can point to the fact that intensive processes of molecule association, related to the energy release, occur right after the electron action on the kerosene vapors.

Some experimental results of the initiating of gaseous fuel combustion are presented above. The combustion of condensed fuels is of significant interest in practice. We checked the possibility to initiate the combustion of a fine-dispersed fuel by the example of a carbon-oxygen mixture. The experiment scheme was the following. The prepared fine graphite powder (5 micron and less) was set on a diaphragm dividing the working volume and the oxidizer capacity. The diaphragm was broken at the start; the powder was carried away by the oxygen stream, mixing with the gas. Fig. 9 shows the dependence of the sodium doublet on time. It is seen that the reaction is initiated right at the moment of the gun connection, and continues much longer than the reactions in a homogeneous medium. The reason of the instant intimation of the reaction may be the fact that the graphite particles are charged up to a high potential, which causes the drastic decrease or disappearance of an energy barrier of the initiation of the combustion reaction on particle surfaces. The other explanations may occur, too. This issue must be studied. The reaction time increased, apparently due to the fact that the reaction occurs on the particle surfaces, not in the whole volume.

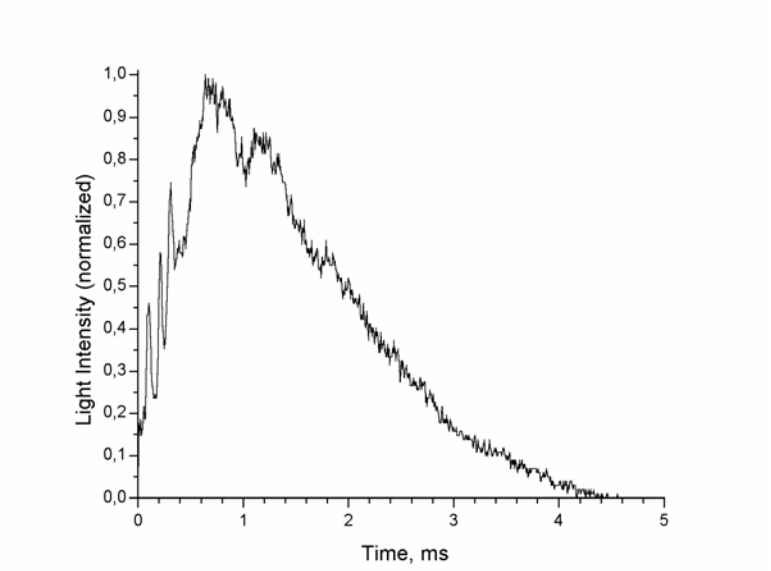

Fig. 23. The intensity of sodium doublet is depending on time for dredge of graphite particles in oxygen.

II.4 Initiation of combustion in in a free supersonic stream of a combustible mixture oxygen and air.

Fig. 24. Picture of the facility. *1* – body, *2* – units of optical windows fastening, *3* – vacuum valve, *4* – objective lens, *5* – turn mirror.

The facility shown on Fig 24 is intended to demonstrate the combustion reaction initiated by an electron beam in a free supersonic stream of a combustible mixture, M = 5, stagnation temperature is up to 300 K, stagnation pressure is no more than several bars.

The functional diagram is shown in Fig. 25, inessential details are ignored. The facility contains a bottle (1) with the mixture closed with electric valve *2*. In the bottom of body *11* (in Fig. 24 designated as *1*) there is supersonic nozzle *3*. The electron beam axis is normal toward the stream direction (*4*, the beam cross section is schematically shown in yellow). The electron gun is situated on the invisible side of the body (Fig. 24). Inside the body there is a couple of mirrors *6* in such a manner that the position *h* of observation point 5 can be changed about the nozzle cut. The mirrors are necessary, since windows *7* are not big enough (120 mm). The intensity radiation was registered for the line produced by monochromator *9* with the aid of photo detector *10*.

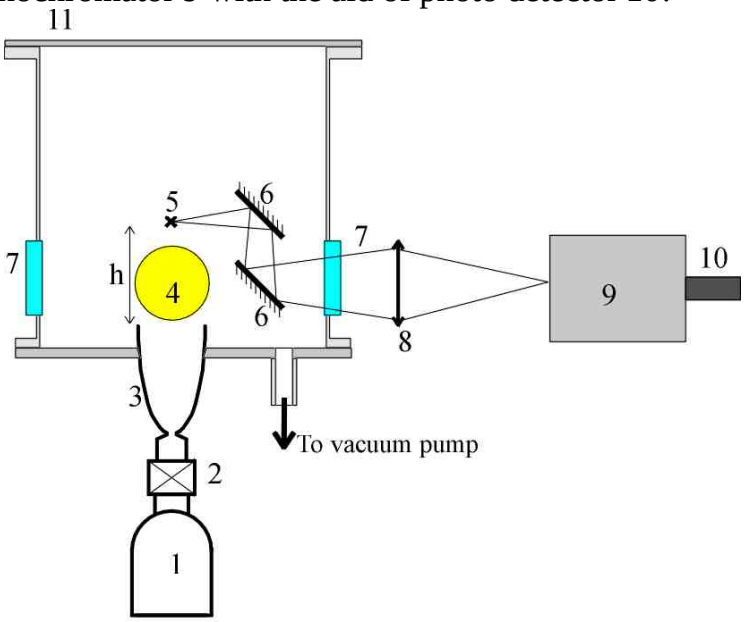

Fig. 25. Facility diagram.

The process cycle of the facility is the following. The facility was pumped out to ~1 Pa , and the bottle was filled with the mixture. Than, valve 2 was opened with the aid of the impulse generator, upon the stream settling, the electron gun was initiated. The radiation intensity, electron current passing through the stream, and the gas pressure ahead of the nozzle critical section were measured. The valve started to open 7 microseconds after the current impulse was sent, and 5 microseconds later the stream was settled, and the gun was started at this moment.

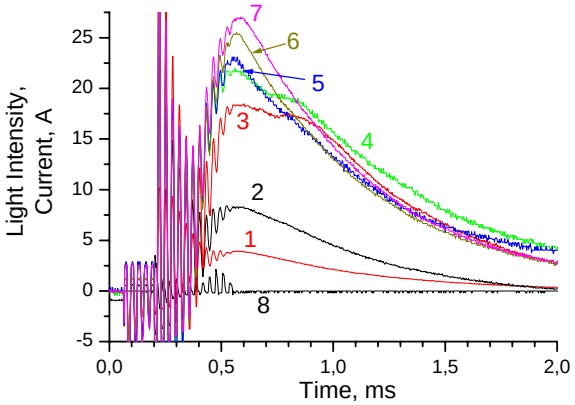

Fig. 26. The luminescence intensity of a CH line with the different concentrations of the natural gas (*1 – 7*), and the electron current value on the collector, depending on time.

Under study was the combustion initiated in the stream of oxygen-natural gas mixture of different concentration. The time dependencies of the luminescence intensity of the CH lines in the region 430 are given in Fig. 26. The mixture pressure in the bottle was set on .3 MPa, the following concentrations of the natural gas in oxygen are reflected by curves: *1* – 80%, *2* – 68%, *3* – 43%, *4* – 33%, *5* – 24%, *6* – 14%, *7* – 7%. The curve *8* corresponds to the electron current passing through the stream and gathered into the collector.

The observation point is situated at the distance of h = 170 mm (Fig. 25). During the work of the gun, the signal from the photodetector contains also an interference, up to about 0.5 ms. During the same time period, one can see the increasing luminescence intensity. Then the signal either falls down monotonically, or (in cases 3 and 4) we could see a plateau of short duration, and then the luminescence intensity falls down. This can be interpreted as follows. The electron beam initiates the combustion reaction in the natural gas in any case, this is proven by the fact that the CH line intensity increases during the gun operation and falls down quite slowly after the operation end. The decrease of the line intensity is apparently associated with the fact that the reaction intensity reduces. It should be taken into account that the time during which the stream passes the way from the nozzle to the observation point, is about 300 microseconds. In two cases one can see some delay (about 300 microseconds) in the radiation intensity drop. Here the mode seems to approach the self-sustaining mode, when the front of the reaction moves upstream with the speed close to the stream speed. In some experiments the reaction front moved upstream and penetrated inside the bottle with the mixture, which resulted in an explosion. The experiments performed allow assuming that electron-beam beaming of the combustible mixture of the natural gas and oxygen may initiate the combustion reaction. It is conceivable that this method can be used in the detonation engines to stabilize the detonation front.

II.5 Initiation of nature gas combustion in a free supersonic air stream.

New setup for this works was built. General view of this setup is shown on the Fig. 27. Fig. 28. shows the scheme of the setup in middle section.

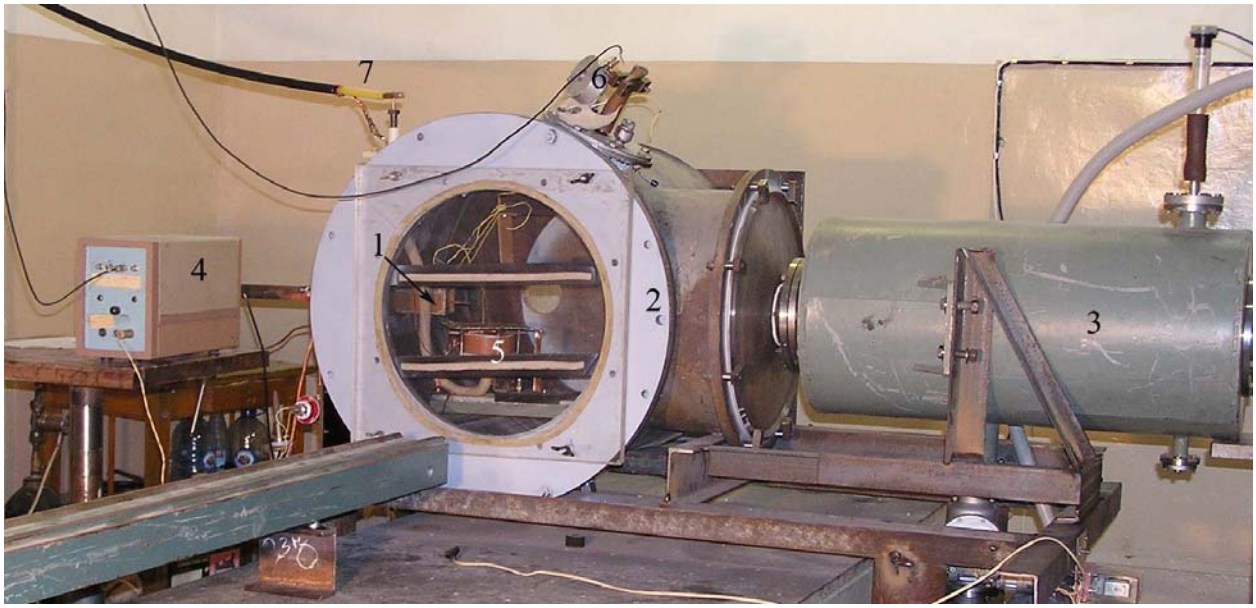

Fig. 27. Common view of the setup. 1 – supersonic nozzle, 2 – working chamber, 3 – vacuum receiver, 4 – electromagnetic valves start device, 5 – electron gun, 6 – Rogovsky coil, 7 – electron gun feeding.

Before the start, the working volume of the facility was pumped out to the pressure of about 3 Pa, the air reservoirs (*5*) and combustible gas (*6*) can be filled up to 1MPa. In the experiments the natural gas was used as a fuel. Electromagnetic valves were opened by the pulse current supplied from the generator *4*. The nozzle is of a square cross section, the critical cross section area is 10×10 mm^2, 50×50 mm^2 at the cut, geometrical Mach number is M = 5 (for air). The tube *11* is of the circle cross section with the inner diameter of 4 mm. Fig. 29 shows the pressure pulses for the natural gas (*1*) and air (*2*). The air pressure was measured in the nozzle settling chamber, the natural gas pressure – at the tube's exit. The electron gun was started at the 18th microsecond, when the pressure in the settling chamber reached its maximum.

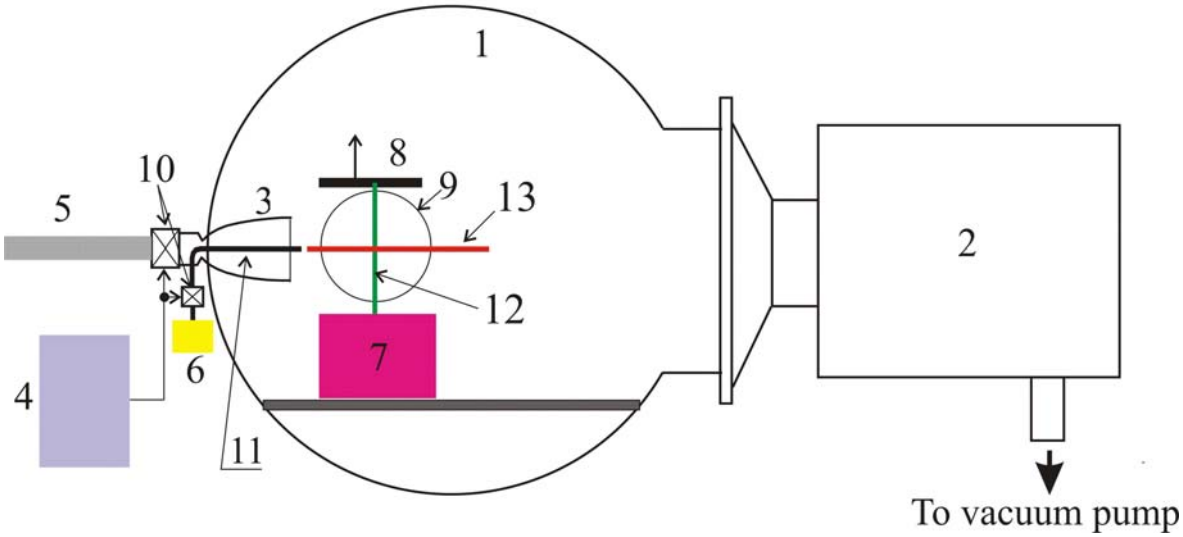

Fig. 28. Scheme of the setup. *1* – working chamber, *2* – vacuum receiver, *3* – supersonic nozzle, *4* - electromagnetic valves start device, *5* – receiver for pressed gas used for nuzzle feeding, *6* - receiver for inflammable gas, *7* – electron gun, *8* – electron current collector, *9* – optical window, *10* – electromagnetic valves, *11* – tube for inflammable gas, *12*, *13* – orientations of photoscanner's slit.

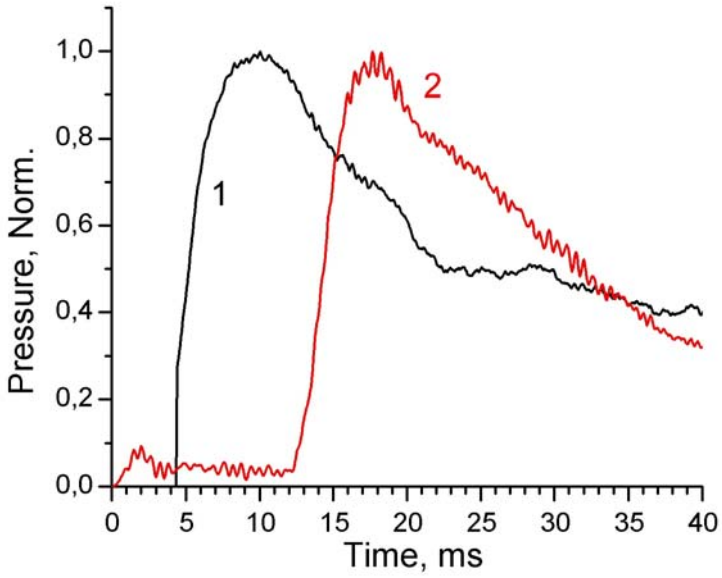

Fig. 29. Time dependences of pressure in the tube (*1*) and in the nuzzle prechamber (*2*).

The next Figures demonstrate the photos of the region beamed by the electrons. These photos have been obtained with the shutter open within the whole period of the gun operation. Fig. 30 presents the resting gas (air, ~5Pa) radiation, the stream is absent. The electron source is beneath, from the left one can see the nozzle cut, and a collector – from above. The whole half-space above the gun undergoes the electron beaming.

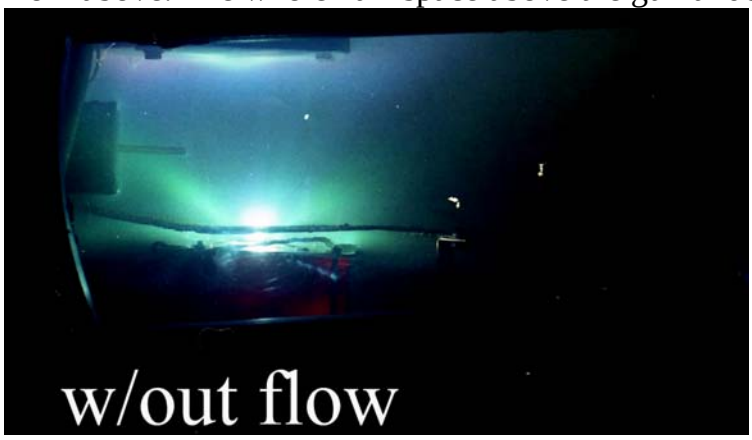

Fig. 30. Resting gas (air) radiation on the e-gun action.

The next three Figures show the pattern of the glowing air stream (the pressure in the settling chamber is 0.4 MPa), natural gas stream (the pressure in the source is 0.4 MPa), and with the simultaneous supply of the air and natural gas at the same pressures. The difference is evident.

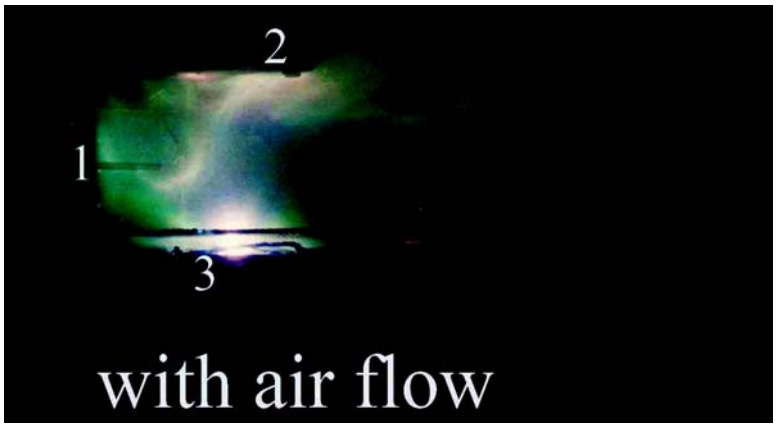

Fig. 31. Lighting of air flow on the e-gun action.

Fig. 32. Lighting of air flow on the e-gun action.

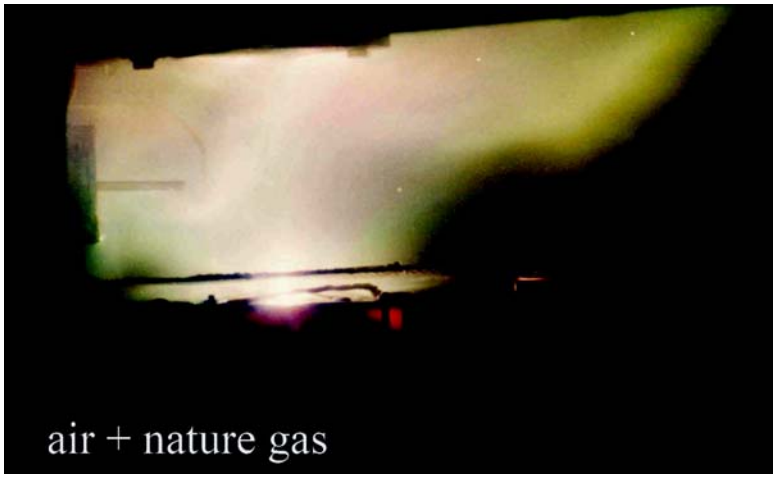

Fig. 33. Lighting from summary gases flow on the e-gun action.

The following two figures demonstrate the speed film frames, one of the air flow under the beam irradiation (Fig.34) and the other of the same flow with the natural gas submitted along its axes. (Fig.36). Scheme of frames is shown on the Fig. 35. The flow parameters were the following: the Mach number (geometrical, for the air) M=5; the nozzle exit size was of 50×50 mm^2; the stagnation temperature was a room one; the total pressure of air was of 0.6 MPa; the total pressure of methane in a receiver - of 0.55 MPa. The natural gas was supplied through a tube of 3 mm inner diameter. The picture frequency was of 31250 frames per second that makes 32 mks per frame.

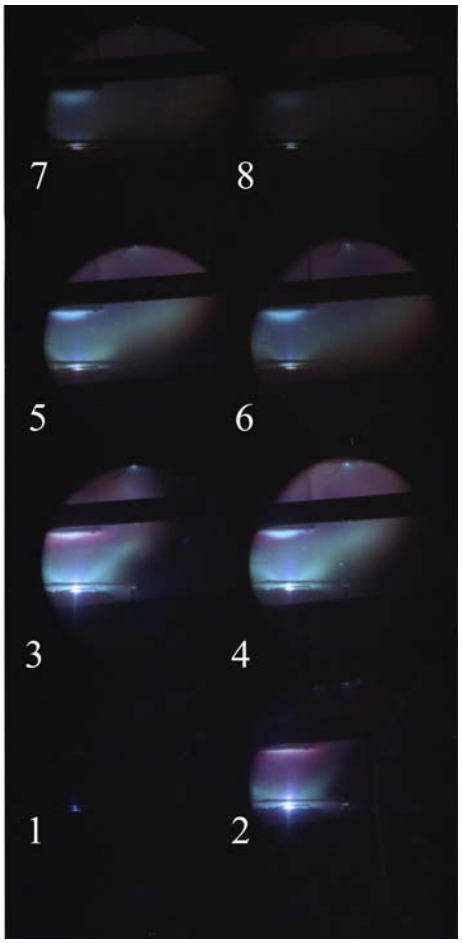

Fig.34. Air flow under the beam irradiation.

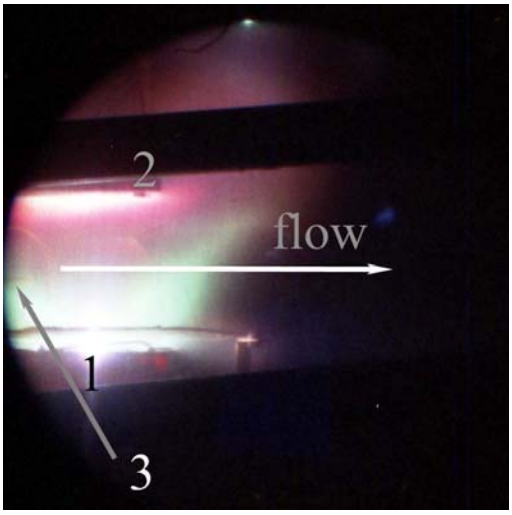

Fig. 35. Scheme of frames. *1*- electron gun, placement of exhaust hole, *2* – collector, *3* – tube for nature gas injection.

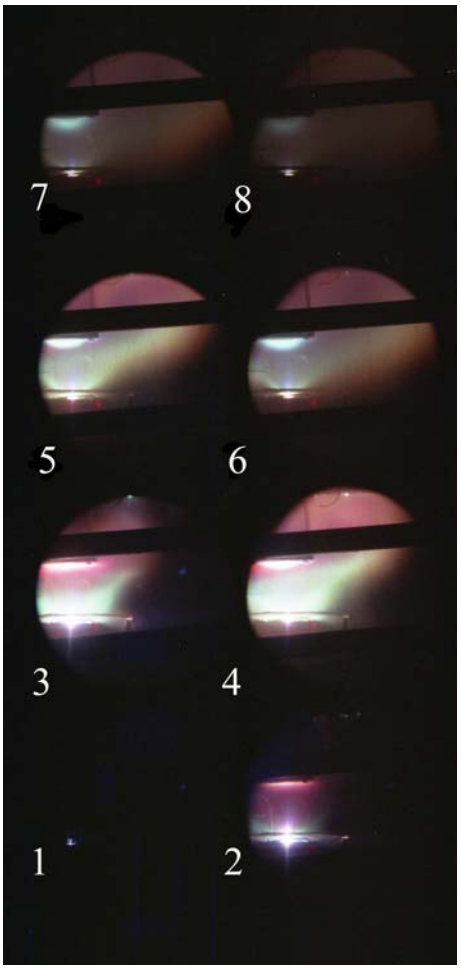

Fig. 36. Air + nature gas flow under the beam irradiation.

The following figures demonstrate the example of photo-scanning patterns obtained at irradiation by electron beams of a rest residual gas (Fig.37) and at irradiation of the air flow with the natural gas submission (Fig.38). The registering of photo-scanning shown in these figures was performed as the slit was arranged inline the beam spreading along the line connecting the gun exit orifice with the collector (as shown on Fig. 28, *12*).

The collector is situated at the top of the figures the electrons moving top down. The distance is shown in millimeters. .

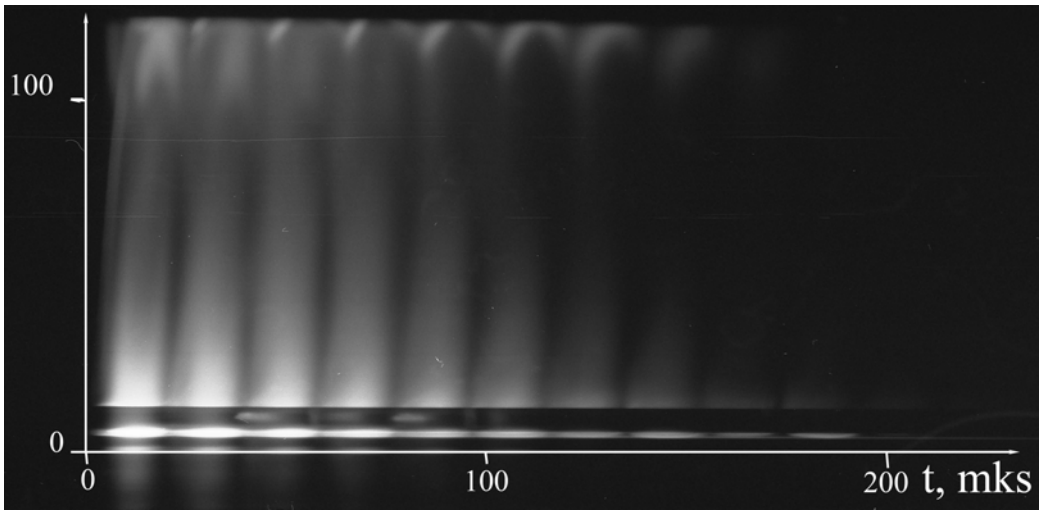

Fig. 37. Photo-scanning patterns obtained at irradiation by electron beams of a rest residual gas

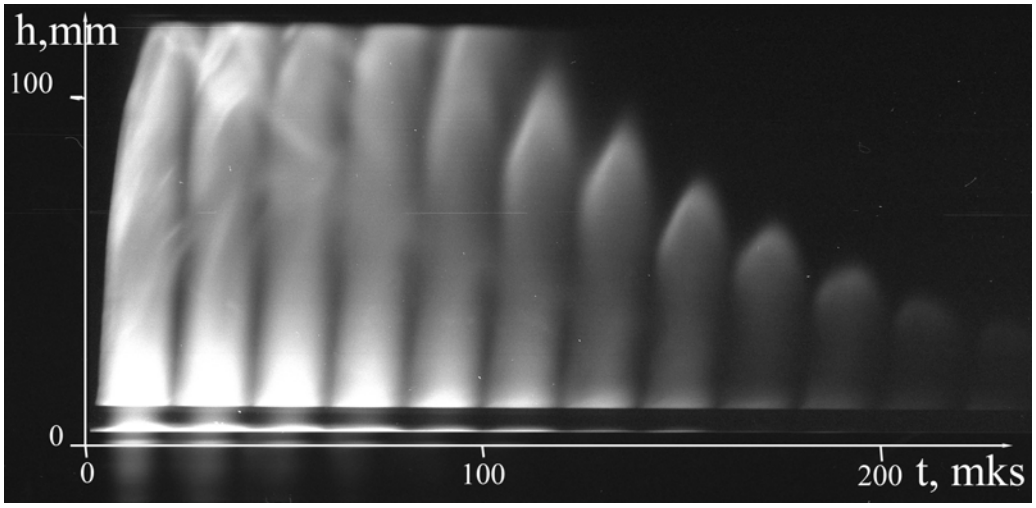

Fig. 38. Photo-scanning patterns obtained at irradiation by electron beams of the air flow with the natural gas submission

The comparison of the photo-scanning imagoes shows that in the case when the residual gas was irradiated by the beam the electrons reach the collector in each impulse, and in the case of flow irradiation the first five impulses reach the cathode while the rest of impulses having less energy are absorbed by the flow. Besides the spread time in the second case is larger. Some structure is observed in the flow (fig.38) which is probably connected with the propagation of combustion front crosswise the flow. Fig 39. shows the photo-scanning obtained at lengthwise position of the photo register slit relative to flow direction (horizontal line *13* on the Fig. 28).

It should be noticed that at the upper photos the radiation of gas was registered under the beam radiation. The lightening caused by chemical reaction is much less so that it could not be observed in a photo. The radiation caused by natural gas oxidation reaction was registered through monochromator using a secondary emission photocell. The monochromator was adjusted to the emission band of radicals *CH* (of about 430 nm). This band is common for the hydrocarbon flame. The experimental results are shown in Fig.

40. The measurements were made in 6 points along the flow axis beginning with the point located practically at the edge of the tube submitting natural gas. The distance between test points makes about 100 mm. The diagrams make it evident that the reaction time is much larger then the time of gun action. (less then 0.2 ms).

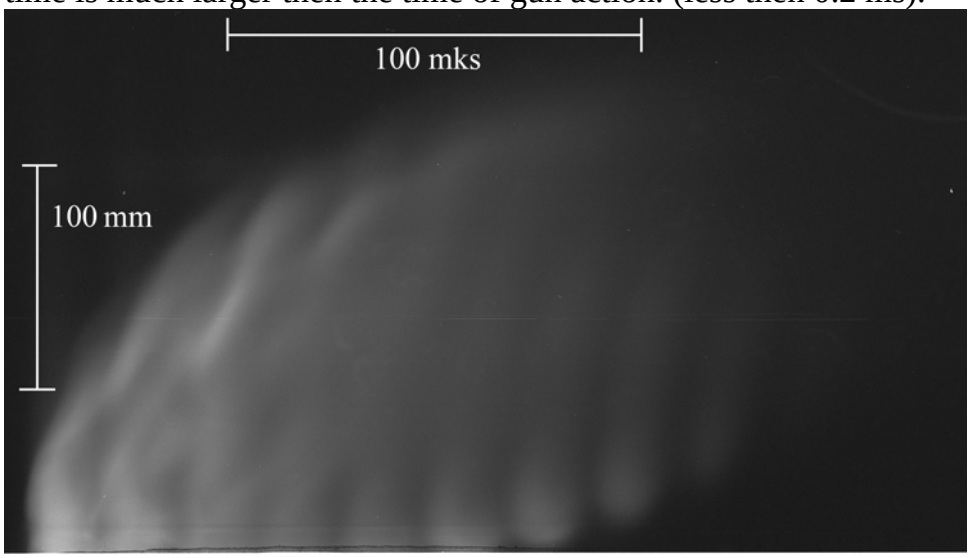

Fig. 39. The photo-scanning obtained at lengthwise relative to flow slit position.

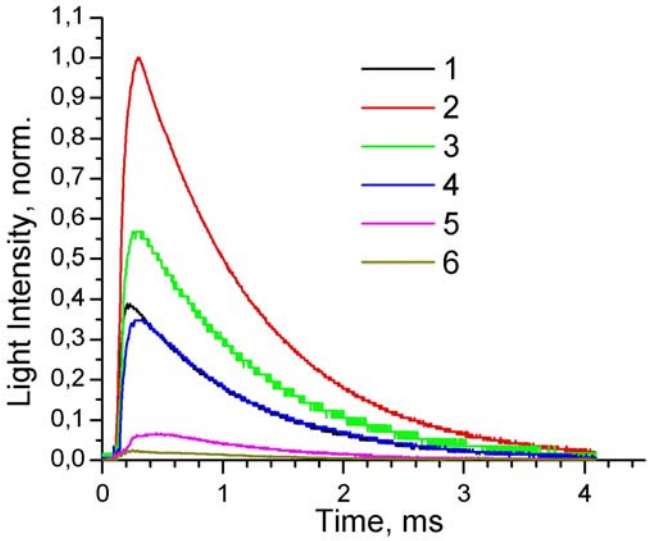

Fig.40. Time dependencies of *CH* irradiation band (about 430nm) intensities normalized by maximum (for all diagrams) value.

In order to make sure that the combustion reaction was initiated by electron beam there was arranged a thermocouple sensor, fabricated from thin (diameter 0.05 mm) wires, at the distance of 250 mm from the nozzle, and its signal was registered with the use of analogous memory oscilloscope having appropriate sensitivity (greater then of a digital one). Fig. 41 demonstrates thermocouple signals in the air flow under irradiation (to the left) and in the same flow with submission of natural gas. The noise signal due to gun operation is observed in both pictures the heat flow being registered only at fuel gas submission.

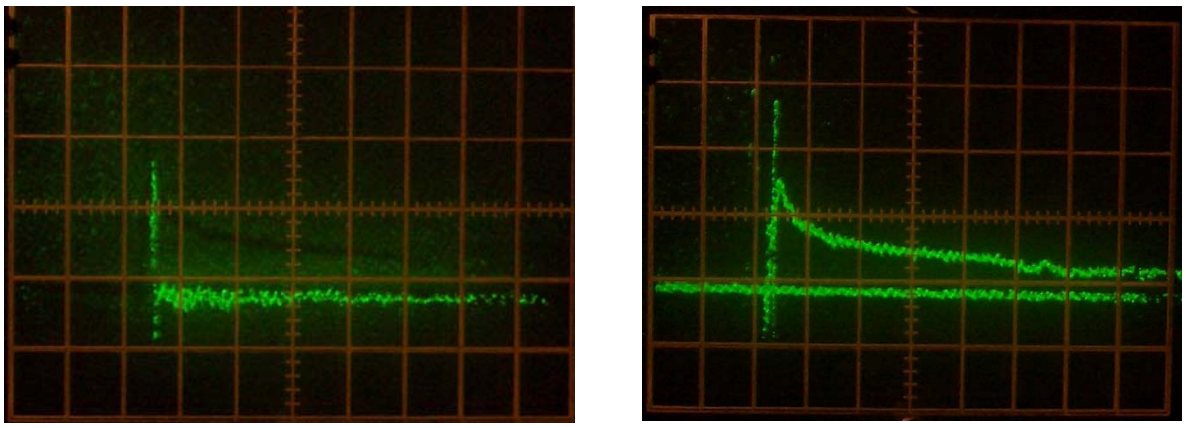

Fig. 41. Signals from thermocouple: left – without nature gas, right – with nature gas injection, time divisions is 5 ms.

The presented results justify that the electron beam may be used to initiate the natural gas combustion in a supersonic air flow. The data available in literature suggest that it is more difficult to inflame the natural gas (methane) in a supersonic flow than any other hydrocarbon. This gives the hope that the proposed means of combustion initiation may be also used at higher values of stagnation temperature and pressure.

II.6 Initiation of nature gas combustion in the channel of constant cross-section.

The model shown in the photo on Fig. 42 has been chosen as a combustion channel. The major reason was that this model was used in the experiments performed for the contract with Boeing Company some years ago. The purpose of these experiments was to study the combustion of the liquid fuel in a supersonic stream with the almost-full-scale parameters. The results of these experiments have been published, among others, in [1].

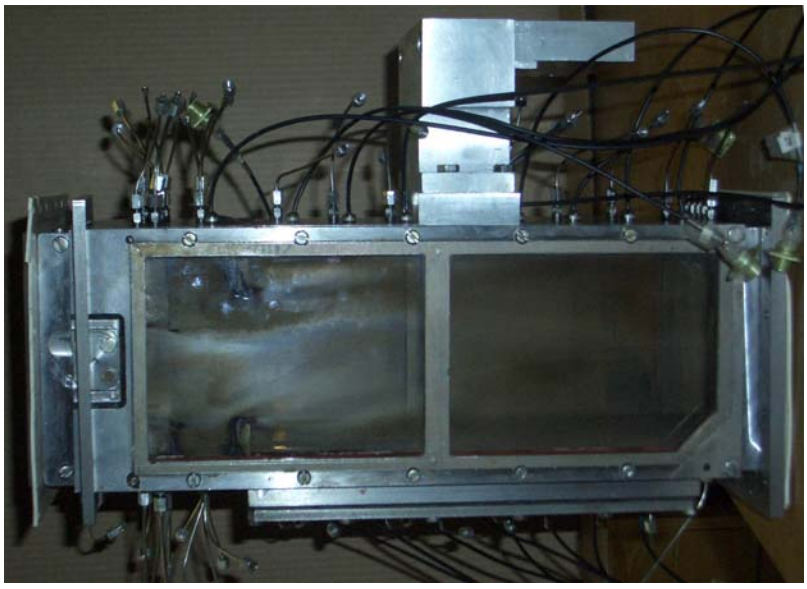

Fig. 42. The combustor channel.

The authors of [1] have agreed to apply the chosen model to carry out the experiments of the combustion initiation with the aid of the electron beam for the project RP0-1393-NO-03. The channel model with the length of about 400 mm has quartz windows for the optical diagnostics, drainage channels to measure the pressure distribution over the walls, in the left bottom and right top angles there are fuel injectors. The bottom wall has a window of 55×220 mm^2, the electron gun will be installed instead of it.

The physical analog of the electron gun, which will be used in the experiments in the hot-shot wind tunnel IT-302, has been tested in our hot-shot wind tunnel. The photo, Fig.43, shows the location of the gun in the working part. The numbers designate: *1* – electron gun, *2* – adapter for the gun installation onto the place of the bottom window, *3* – nozzle, *4* – current collector.

Fig. 43. The location of the e–gun in the working

The experiments were carried out with the stagnation pressure p^*=0.6 MPa (*1*) and p^*=1 MPa (*2*), which is maximum allowed in our facility, stagnation temperature was T^* =300 K, Mach number M=5. While electron beaming the stream, the electron absorption in the gas depends on the gas density. That is why our facility simulates the conditions of the interaction between the electron beam and stream with, for example, the following stagnation parameters: p^*=10 MPa and stagnation temperature T^* =3000 K, with the same Mach number. In Fig. 44 we show the dependence of the current passed through the stream.

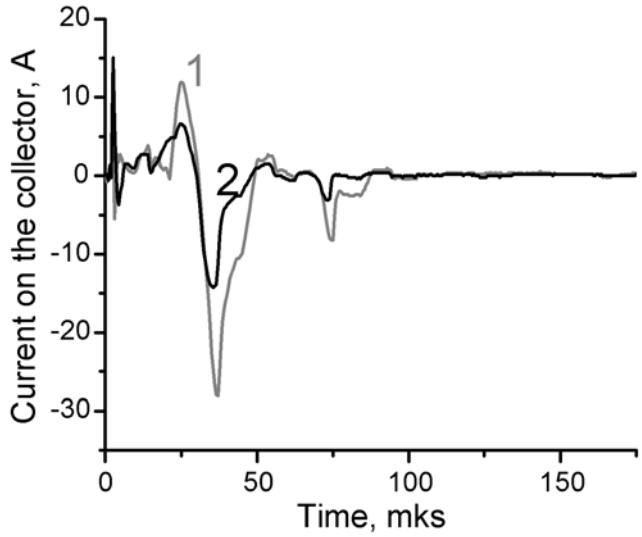

Fig.44. Current on the collector at different stagnation pressure:
1 – p^*=0.6 MPa, *2* – p^*=1 MPa.

Hence, the combustion chamber for the previous tests has been mounted inside the vacuumed working part of our wind tunnel, as it is shown in Fig. 45. The chamber cross section is constant of 100×100 mm^2, the impulse air flow inflows from the left. It has the cross section of 50×100 mm^2 and is formed by the Laval rectangular nozzle with a slot critical cross section of 2×100 mm^2. M number of the nozzle is 5. The air comes from the constant-volume receiver through a valve, thus, the pressure impulse has quite a short amplification front followed by the smooth pressure drop. The fuel (natural gas) is also supplied from the constant-volume receiver through the valve into the stream through the system of distributed holes in the combustion chamber walls. Both valves open simultaneously. The gas pressure in the receivers may run up to 1.5 MPa. The combustion chamber has a special configuration to organize fuel and air mixing. The numbers designate: *1* – slot nozzle, *2* – combustion chamber, *3* – natural gas duct, *4* – full head tube, *5* – the unit of pressure strain gages, *6* – ignition system.

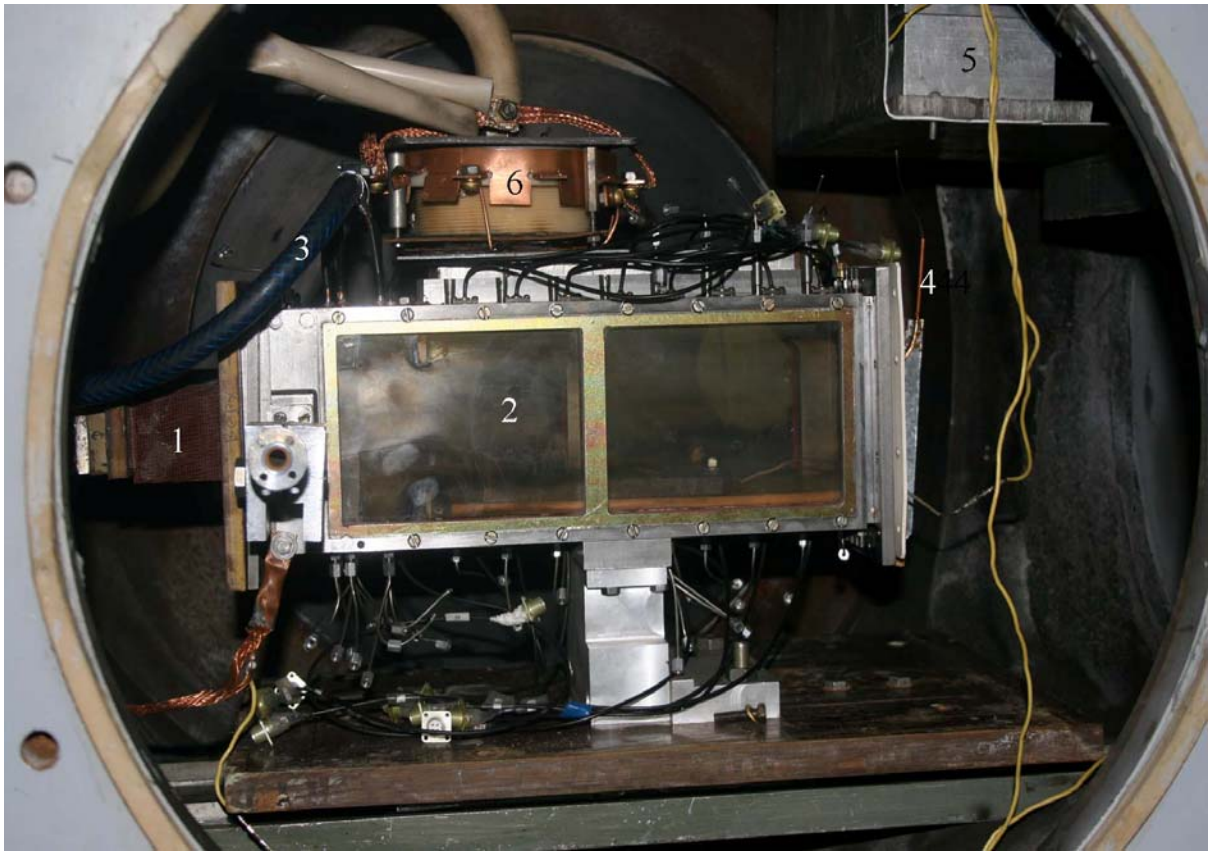

Fig.45. Common view of the set-up. 1 – slot nozzle, 2 – combustion chamber, 3 – natural gas duct, 4 – full head tube, 5 – the unit of pressure strain gages, 6 – ignition system.


Fig. 46. Stream with the combustion initiation.

The following Fig. 46 demonstrates a photo of the stream with the combustion initiation. Strong irradiation results not from the combustion reaction, but from the irradiation of the electron-beamed gas stream, since the brightness of the glow is almost

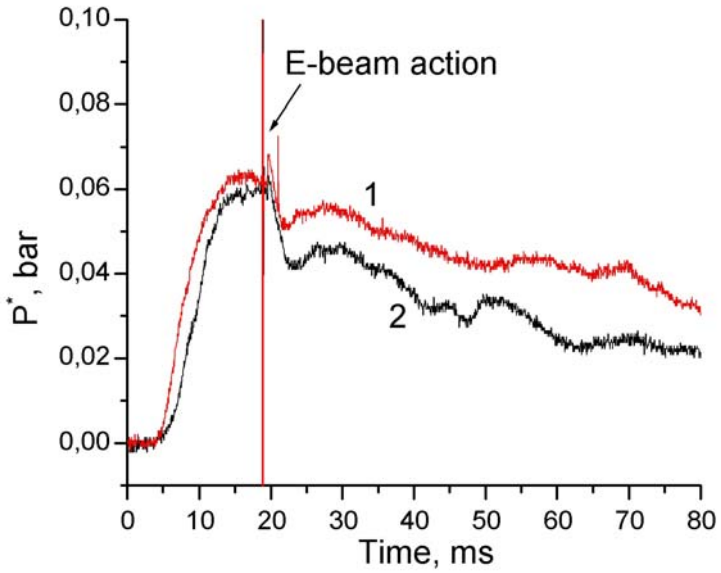

Fig. 47. The typical time dependences of the velocity head.

The reducing stagnation pressure registered by the head gage at the combustion chamber exit is an objective evidence of the combustion in the stream. Fig. 47 shows the typical signals from the pressure gage, which measures the velocity head. The curve *1* has been obtained without natural gas supplied into the combustion chamber. The graph presents the moment of the combustion initiation. With the delay being under 5 ms, one can see the pressure reduce, caused by the fact that the gas region, heated by the electron beam, reaches the gage. Then the pressure becomes the same as it is without stream beaming. In the case of the natural gas supply into the stream (curve *2*), we observe the evident pressure reduce relative to the pure air stream from the combustion initiation moment, plus the same delay of 5 ms to the end of observation. We suppose this is caused by the successful initiation of the combustion reaction of the natural gas in the stream. The result has been obtained at the stagnation temperature of 300 K and stagnation pressure of 1.1 MPa. At higher stagnation pressure and temperature, which are typical for the nature conditions, the combustion initiation is believed to be easier.

The experiment results permit to conclude the following:

1. The combustion of hydrocarbon fuel vapors in oxygen and air can by initiated with the aid of the electron beam;
2. The inductance time of this reaction is in any case not longer than the hydrogen combustion reaction.
3. Quite sophisticated combustion kinetics is observed.
4. The combustion of heterogeneous mixtures can be initiated by the electron beam, too, which was demonstrated by the example of a graphite powder suspension in oxygen.
5. The combustion of nature gas in a supersonic air flow can be initiated by the electron beam.

Theoretical part.

Estimation of Possible Kinetic Combustion Machinery of Oxygen-Hydrogen Mixture under Influence of Low Energy Heavy-Current Electron Beam (about 10 keV), Based on Semi-Empirical Representations

Influence of electron beam with electrons energy ~10 keV on chemical reactions running at gas-core area practically is explored in small extent. On the one part, such electrons are faster then thermal electrons and electrons, received at gas-discharge plasma, but on other part this electrons are slower in comparison with relativistic electrons in beams, generated at famous electron guns. It is well known, that electrons are able to establish effectively inner degrees of reagents freedom in considered energies area and first of all oscillating degrees, and that must lead to increase chemical reactions processing rate, for example, such as hydrocarbon fuels combustion. However, such reactions have chain nature, and the result of cathode beam influence on this reactions progress is unknown.

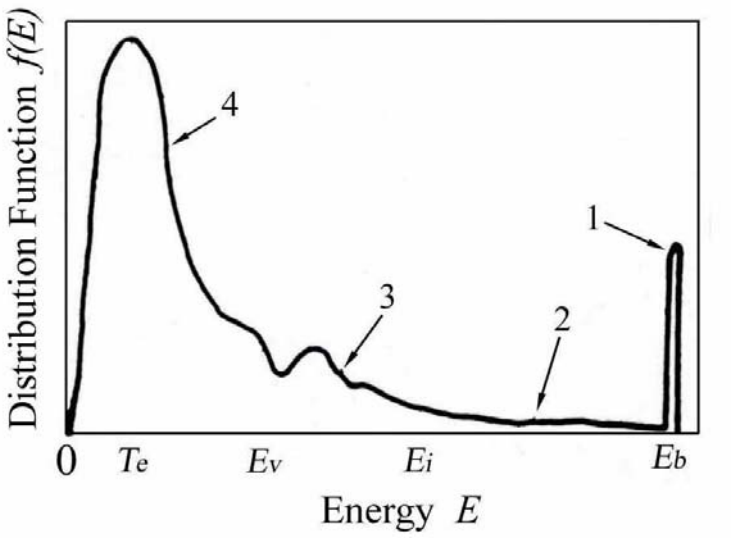

Fig. 48.

Principal idea of theoretical study of similar problems is determination of electrons degradation spectrum, and it is autonomous, very difficult problem also. However, gathered calculation experience of electron distribution function by energies at cathode beams interaction with plasma indicates that primary electrons lose energy at ionization processes very fast and certain spectrum becomes established, which qualitative view is shown on Fig. 48 taken from review [2]. Vast majority of electrons which are able to stimulate chemical reactions stands at maximum region of distribution function density and can be described approximately by Maxwell distribution function, but then issue of its starting density and temperature estimation remains open. These parameters are considered to be known and defined by experiments in mathematical model represented below. It is supposed further, that reaction goes concurrently at full capacity and diffusion processes are neglected.

In this case system of kinetic equations can be written

$$dn_i / dt = \sum_j \beta_{ij} r_j \qquad (1),$$

where $r_j = k_f \prod_{i(j)} n_i - k_r \prod_{i(j)} n_i$ is effective velocity of elementary reaction j; k_f и k_r are velocities constants of direct and reverse reactions; first product is related to all particles i reaction reagents, second – resultants. β_{is} - element of matrix of reaction mechanism stochiometric coefficients, at that, the coefficients from the reaction resultants side are written with symbol (+), and coefficients from the reagents side are written with symbol (-).

System (1) is complemented with system of equations which represent conservation laws for medium energies of reacting components at multigroup temperature approximation: unexcited molecules and atoms are characterized by unified forward temperature T_0; oscillatory excited molecules – temperature T_v; electron excitation at atoms and molecules- T_{e*}; electrons - T_e. At balance relationships exchange of energy for T_{e*}, T_v occurs as a result of non-elastic collisions and T_e, T_0 are in need to take account of exchange of energy at particles elastic events in addition. Then desired system of equations will be written

$$\begin{aligned}
&\frac{d}{dt}\left(\frac{3}{2}kn_eT_e\right) = \omega_{ei} - \dot{\omega}_{ej} \\
&\frac{d}{dt}(c_\upsilon n_0 T_0) = -\omega_{ei} - \dot{\omega}_{0j} \\
&\frac{d}{dt}(c_\upsilon n_\text{v} T_\text{v}) = -\dot{\omega}_{\text{v}j} \\
&\frac{d}{dt}(c_\upsilon n_{e*} T_{e*}) = -\dot{\omega}_{e*j}
\end{aligned} \qquad (2),$$

where $\omega_{ei} = \sum_i \frac{2m_e}{m_i}\frac{3}{2}k\nu_{ei}n_e(T_0 - T_e)$, ν_{ei} – rate of electron collusion with all particles, taking part in reaction mechanism (with the exception of electron); $\dot{\omega}_{kj} = \sum_j \Delta H_j^k r_j$ – heats of corresponding reactions $(k = 0, \text{v}, e*)$, that were summed by all elementary reactions j: c_υ – heat capacity at constant volume, n_0, n_v, n_{e*} – total concentrations of all particles having temperature T_0, T_v, T_{e*} correspondingly.

Given mathematical model was developed for estimation of possible elementary kinetic reactions function at experimental research of combustion processes, stimulated by heavy-current cathode beam of low (~ 10 keV) energy [3]. Preliminary results of modeling for hydrogen oxidation reaction are represented below.

Experimental reaction mechanism included following set of elementary reactions.

I. Reactions in system $H_2 - O_2$

This reaction mechanism is explored well enough [4], it is represented by following elementary reactions

j	reaction	A_j	b_j	E_j
1	$H_2 + O_2 = 2OH$	$1{,}7*10^{13}$	0	47,78
2	$H + O_2 = OH+O$	$1{,}21*10^{17}$	-0,91	69,1
3	$O + H_2 = OH + H$	$1{,}5*10^{7}$	2,0	31,6
4	$OH + H_2 = H_2O + H$	$1{,}08*10^{8}$	1,6	13,8
5	$OH + OH = H_2O + O$	$1{,}5*10^{9}$	1,14	0

6	$H + H + M = H_2 + M$	$9,7*10^{16}$	-0,6	0
7	$H + OH + M = H_2O + M$	$1,47*10^{23}$	-2,0	0
8	$H + O_2 + M = H_2O + M$	$2,0*10^{18}$	-0,8	0
9	$H + HO_2 = OH + OH$	$1,5*10^{14}$	0	4,2
10	$H + HO_2 = H_2 + O_2$	$2,5*10^{13}$	0	2,9
11	$H + HO_2 = H_2O + O$	$3,0*10^{13}$	0	0
12	$O + HO_2 = OH + O_2$	$2,0*10^{13}$	0	0
13	$OH + HO_2 = H_2O + O_2$	$2,0*10^{13}$	0	0
14	$H O_2 + HO_2 = H_2O_2 + O_2$	$2,0*10^{12}$	0	0
15	$H + H_2O_2 = H_2 + HO_2$	$1,7*10^{12}$	0	15,7
16	$H + H_2O_2 = H_2O + OH$	$1,0*10^{12}$	0	15,0
17	$OH + H_2O_2 = H_2O + HO_2$			

Constant of reaction rate is determined in the following way:

$k_{f,j} = A_j \cdot T_0^{b_j} \cdot e^{-E_j/T_0}$. $[\mathrm{A}] = \frac{\mathrm{cm}^3}{\mathrm{moll}}$; $[\mathrm{E}] = \frac{\mathrm{kJ}}{\mathrm{moll}}$; $k_{r,j} = \frac{k_{f,j}}{K_{eq}}$

Equilibrium constant $K_{eq}(T_0)$ and heat reactions were being selected from [5],

II Reactions in system of charged particles [6].

II.1. Ionization of atoms and molecules by electron impact.

j	reacton	∇H=I, eV
18	$e + H = H^+ + 2e$	13,5
19	$e + O = O^+ + 2e$	13,6
20	$e + O_2 = O_2^+ + 2e$	12,5
21	$e + H_2 = H_2^+ + 2e$	15,44
22	$e + OH = OH^+ + 2e$	13,18

$k_{f,j}^i = \sqrt{\frac{8kT_e}{m_e}}\sigma_0 e^{-I/T_e}$, $\sigma_0 \sim 10^{-16}\,\mathrm{cm}^2$

$k_{r,j}^i = k_{f,j}^i / K_{eq}^i$

$K_{eq}^i = 4,85 \cdot \frac{g_i}{g_0} T^{3/2} e^{-I/kT}$

$g_{i,}\, g_0$ – statistical weights of ion and atom (molecule) correspondingly, I – ionization potential

II.1. Destruction processes of charged particles.

1.2. Dissociative recombination of electron with ion

$k_{f,j}^{ei}(T_e, T_0) = \frac{A}{\sqrt{T_e}, T_0}$.

j	reaction	A	ΔH, eV
23	$e + O_2^+ \rightarrow O + O$	$2{,}0\cdot10^{-7}$	-10,6
24	$e + H_2^+ \rightarrow H + H$	$3{,}0\cdot10^{-8}$	-10,88
25	$e + OH^+ \rightarrow O + H$	$3{,}0\cdot10^{-8}$	-9,03

1.3. Dissociative electron attachment to neutral particles.

$$k_{f,j}^{e0}(T_e) = \sigma_a(\varepsilon_{\max})\sqrt{\frac{2\varepsilon_{\max}}{m}}\frac{\Delta\varepsilon}{T_e}\exp\left(-\frac{\varepsilon_{\max}}{T_e}\right)$$

ev j	reaction	$\varepsilon_{\max}$, eV	$\sigma_a(\varepsilon_{\max})$	$\Delta\varepsilon$	ΔH,eV (T_e=1eV)
26	$e + O_2 \rightarrow O^- + O$	6,7	10^{-18}	1	2.42
27	$e + H_2O \rightarrow O^- + H_2$	8,6	10^{-18}	2,1	2,6
28	$e + H_2O \rightarrow H^- + OH$	6,5	$7\cdot10^{-18}$	1	2,16

II. 2. Ions destruction.

2.1. Ion – ion recombination.

$$k_{f,j}^{ii} = \frac{8\pi e^6}{27}\frac{\bar{\upsilon}_{om}}{(kT_i)^2\lambda_i},$$

where $\bar{\upsilon}_{om} = \sqrt{\frac{8kT_i}{\pi\mu_{ik}}}$; $\lambda_i = \frac{1}{\sum_k n_k Q_{ik}\sqrt{m_i/m_k}}$ - average length of ion free path. Collisions sections $Q_{i0} = 10^{-13}/\sqrt{T_i}$; $Q_{ii} = \frac{1}{4}Q_{ie}$.

j	reaction	ΔH,eV
29	$H^+ + H^- \rightarrow 2H$	-12,85
30	$H^+ + O^- \rightarrow H + O$	-12,33
31	$O^+ + O^- \rightarrow O$	-12,59
32	$H_2^+ + H^- \rightarrow H_2 + H$	-14,59
33	$H_2^+ + O^- \rightarrow H_2 + O$	-14,1
34	$O_2^+ + H^- \rightarrow O_2 + H$	-11,35
35	$O_2^+ + O^- \rightarrow O_2 + O$	-10,85

2.2. Destruction of negative ions with electron restoration.

j	reaction	k_{fj}^{i0}, cm^3/s	ΔH,eV
36	$O^- + O \rightarrow O_2 + e$	$2\cdot10^{-10}$	-3,6
37	$O^- + H_2 \rightarrow H_2O + e$	10^{-9}	-3,5

III. Oscillatory excitation of molecules by electron impact.

Processes associated with vibrational transitions of lower electron state molecules(0 – 1) are considered in this part and further. Oscillatory energy ε_v can be represented from this sight as

$\varepsilon_v(T_v) = \frac{h\nu}{e^{h\nu/kT_v} - 1} = \frac{\omega_e}{e^{\omega_e/kT} - 1}$, where ω_e – oscillatory quantum of mentioned transition [6]

j	reaction	k_{fj}^{ev}, cm^3/s	$\Delta H = \omega_e$, eV
38	$H_2 + e \rightarrow H_2^* + e$	$4{,}5\cdot10^{-10}\cdot(T_v/11600)$	0,33
39	$H_2O + e \rightarrow H_2O^* + e$	10^{-10}	0,5
40	$O_2 + e \rightarrow O_2^* + e$	$6{,}0\cdot10^{-10}\cdot(T_v/11600)$	0,09
41	$OH + e \rightarrow OH^* + e$	$3\cdot10^{-10}$	0.5

IV. v-T relaxation.

j	reaction	k_{fj}^{vT}, cm^3/s
42	$O_2^* + M \rightarrow O_2 + M$	$10^{-10}\exp(-129\cdot T_v^{-1/3})$
43	$H_2^* + M \rightarrow H_2 + M$	10^{-16}
44	$H_2O^* + M \rightarrow H_2O + M$	$5\cdot10^{-16}$
45	$OH^* + M \rightarrow OH + M$	$10^{-12}\exp(-14\cdot T_v^{-1/3})$

$\Delta H = \varepsilon_v(T_v) - \varepsilon_v(T_0)$

V. Chemical reactions of oscillatory excited particles.

Constant of reaction rate can be represented as [6]

$$k_R(\varepsilon_v) = k_0 \exp\left[\left(-\frac{E_a - \alpha\varepsilon_v}{T_0}\right)\cdot\theta(E_a - \alpha\varepsilon_v)\right].$$

Here α – coefficient of oscillatory energy using E_a – activation energy, $\theta(E)$ – Heaviside function, $k_0 \simeq 10^{-10}$ cm^3/s

j	reaction	E_a,eV	α	ΔH,eV
46	$H + OH^* \rightarrow H_2 + O$	1,85	0,99	1,83
47	$OH + OH^* \rightarrow H_2O + O$	1,52	1	1,48
48	$OH + OH^* \rightarrow H_2O + H$	1,85	0,9	1,65
49	$O + H_2^* \rightarrow OH + H$	0,43	0,31	0,08
50	$H + H_2^* \rightarrow H_2 + H$	0,33	0,35	0
51	$OH + H_2^* \rightarrow H_2O + H$	0,25	0,24	-0,64
52	$H + H_2O^* \rightarrow H_2 + OH$	0,98	0,75	0,6
53	$OH + H_2O^* \rightarrow H_2O_2 + H$	3	0,88	2,6
54	$OH + H_2O^* \rightarrow H_2 + HO_2$	3,3	0,73	2,1
55	$HO_2 + H_2O^* \rightarrow H_2O_2 + OH$	1,3	0,86	1,1

Reactions with participation of electron-excited particles are not considered. Thus, following particles participate in hydrogen oxidation mechanism with the collaboration of cascade electrons, occurred as a result of cathode beam influence (i=20):
H_2, O_2, H, O, OH, H_2O, HO_2, H_2O_2, e, H^+, O^+, H_2^+, O_2^+, OH^+, O^-, H^-, H_2^*, O_2^*, H_2O^*, OH^*.

Following initial conditions were specified for stochiometric mixture:
$n_{O_2} = 5 \cdot 10^{16}$ cm^{-3}, $n_{H_2} = 10 \cdot 10^{16}$ cm^{-3}, $T_0 = 300K$
Initial temperature and density of electron gas: $T_e = 10^4 K$, $n_e = 15 \cdot 10^{14} cm^{-3}$
Initial system of equations

$$\frac{dn_i}{dt} = \sum_j \beta_{ij} r_j$$

$$\frac{d}{dt}\left(\frac{3}{2} k n_e T_e\right) = \omega_{ei} - \dot{\omega}_{ej}$$

$$\frac{d}{dt}(c_\upsilon n_0 T_0) = -\omega_{ei} - \dot{\omega}_{0j}$$

$$\frac{d}{dt}(c_\upsilon n_\nu T_\nu) = -\dot{\omega}_{\nu j}$$

was deprived of dimension by initial parameters, moreover time scale is determined by maximum value of r_j. The explicit difference scheme was used for solution.

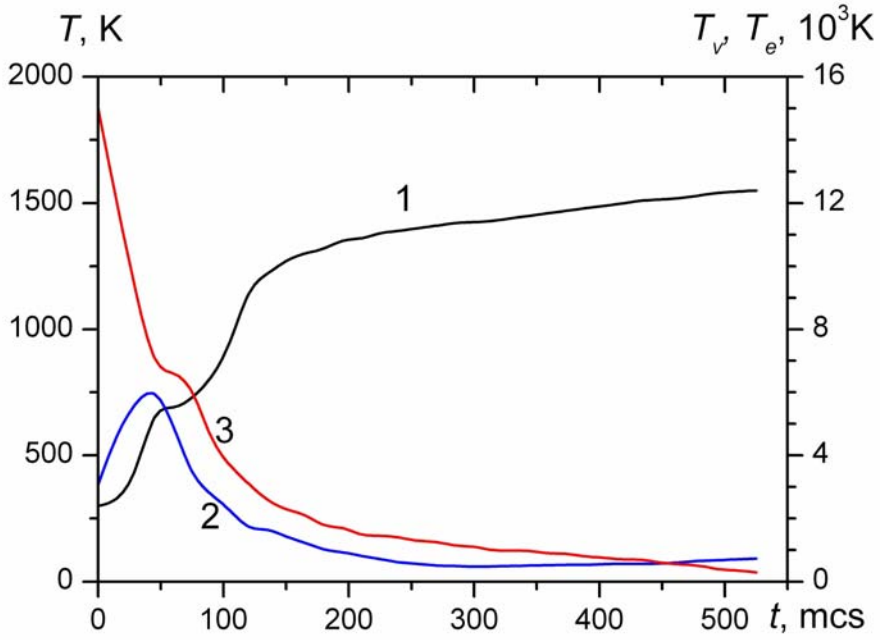

Fig. 49. Time dependences of: *1* – gas temperature T_0, *2* – vibration temperature T_v, *3* – electron temperature T_e

Results of computations are represented on Fig. 49 and Fig. 50 partially. Formation processes of positive and negative ions leading to fast electrons temperature reduction were dominating on initial stage of reaction. Ion recombination is passing at the same time and results in release of great amount of energy and molecules oscillatory excitation. Intensive gas temperature growth is observed on this phase. Seemingly this phase is trigger starting mechanism of main oxidation reaction.

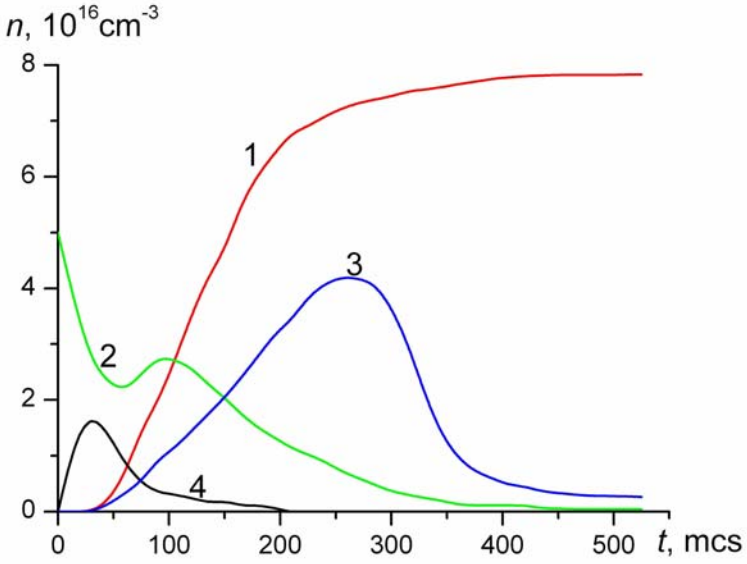

Fig. 50. Time dependences of: *1* – H_2O, *2* – O_2, *3* – OH, *4* – O_2^+

Results of this project was published: [3,8,9], one report accepted to 8th ISAIF and another report submitted to 43rd AIAA/ASME/SAE/ASEE Joint Propulsion Conference & Exhibit.

Conclusions.

1. The possibility of electron-beam initiation of the hydrogen and hydrocarbon fuels combustion in oxygen and air has been demonstrated for different mixture concentrations.
2. It is demonstrated that the combustion of the methane in air stream with M = 5 can be initiated.
3. The kinetics of the reaction initiated by the electron beam differs from the kinetics of the reaction initiated by the traditional method – with the aid of a thermal source. The semiempirical kinetic model is created. On an example of response of oxidation of hydrogen the basic gears of responses going at electron – beam effect are detected.

Our schedules for the future are next. We are searching a financial support for continues this work now.

References

1. M.A. Goldfeld , A. A. Mishunin and A. V. Starov, A. B. Mathur, *Investigation of Hydrocarbon Fuels Combustion in Supersonic Combustor* Institute of Canoga Park, CA 91309-7922, USA AIAA Paper 2004-3487, 11p.
2. Konovalov, V. P., and Son, E. E., *Degradacionnye cpectry elektronov v gazah. Himija plazmy*, Atomizdat, Moscow, 1985, pp 194 – 227 (in Russian).
3. Golovnov I. A., Pozdnyakov G. A., The Observation of the Combustion Initiated by a Free Electrons Cloud, // Proc. of the AIAA/CIRA 13th International Space Planes and Hypersonics Systems and Technologies, AIAA 2005-3426, Capua, Italy, 16-20 May, 2005
4. Baulch D. L., et al., *Evaluated Kinetic Data for High Temperature Reactions, Vol. 1: Homogeneous Gas Phase Reactions of the H_2-O_2 System,* Butterworths, London, 1976.
5. Glushko V. P. (ed), *Termodinamicheskie* svojstva *individual'nyh vezhestv. Vol.2*,Izd. AN SSSR, Moscow, 1962 (in Russian).
6. Rusanov, V. D., Fridman, A. A. *Fizika himicheski aktivnoj plazmy*, Nauka, Moscow, 1984, p 415.
7. Radtsig A. A., Smirnov B.M., *Spravochnik po atomnoj i molekuljarnoj fizike*, Atomizdat, Moscow, 1980 (in Russian).
8. Katsnelson S. S., Pozdnyakov G. A., Estimation of possible kinetic combustion machinery of oxygen-hydrogen mixture under influence of low energy heavy-current cathode beam (about 10 keV), based on semi-empirical representations, // Proc. of the AIAA/CIRA 13th International Space Planes and Hypersonics Systems and Technologies, AIAA 2005-3427, Capua,Italy, 16-20 May, 2005
9. Katsnelson S. S., Pozdnyakov G. A., Initialization of combustion processes in hydrogen-oxygen mixtures under influence of low energy heavy-current cathode beam (about 10 keV) // Combustion, Explosion and Shock Waves (in printing)